INTER-AMERICAN TROPICAL TUNA COMMISSION

SCIENTIFIC ADVISORY COMMITTEE

13TH MEETING

(*by videoconference*)
16-20 May 2022

DOCUMENT SAC-13-05 CORR.

IDENTIFYING AND CORRECTING THE PURSE-SEINE FLEET CATCH FOR BIAS CAUSED BY THE COVID-19 PANDEMIC IN 2020-2021

Anandamayee Majumdar, Cleridy E. Lennert-Cody, Mark N. Maunder and Alexandre Aires-da-Silva

CONTENTS

1. Summary 1
2. Background 2
3. Data Exploration and Results 4
4. Statistical Modeling 6
5. Results 9
6. Discussion 11
7. Future Work and Directions 12
8. Conclusion 12
9. References 13
Appendix A: Statistical Modeling 31
Appendix B: Estimates and Proformance Measures 34
Appendix C: Data Sources 41

1. SUMMARY

The IATTC port-sampling data are used to determine the species and size composition of the tropical tuna catch, and therefore play a very important role in the current Best Scientific Estimate (BSE) catch estimation methodology. The COVID-19 pandemic generally limited the ability of IATTC port-samplers to collect data in 2020 – 2021, however, the disruption to data collection was greater in some ports than in others. This may have resulted in bias in the BSE of catch composition for 2020 – 2021 because some fleet segments preferentially unload in specific ports. An increase in the 2020 BSE for bigeye tuna (BET) in floating-object (OBJ) sets in 2020, relative to the previous year (SAC 13-03), despite a decrease in OBJ sets (SAC-13-06), and the marked disparity between the 2020 BSE and the reported catches from observers and logbooks for 2020, contributed to a concern about potential bias in the BSE at the 12th Meeting of the Scientific Advisory Committee. A recent study that applied the BSE methodology to data from 2010 – 2019, after simulating a systematic reduction in port-sampling data to match that which occurred in 2020, showed that bias could occur, but that the bias could be either an over-estimation or an under-estimation (SAC-13 INF-L). Therefore, to address the effect of the systematic loss of port-sampling data in 2020-2021 on the BSE, a spatio-temporal model was developed to estimate the port-sampling catch composition

from observer (logbook) data for catch estimation strata for which no port-sampling data were available. Exploratory analyses showed that observer data (supplemented with logbook data, where necessary) could be used successfully to predict the port-sampling species composition, and that prediction was improved when spatial and temporal covariates were included in the model. The spatio-temporal model performed well in terms of the percent variance explained and normalized prediction error, and the catch estimates from the model were highly correlated with the BSEs for 2010-2019, years for which no systematic data losses occurred. Through simulation, the spatio-temporal model was found to be robust to the type of systematic port-sampling data losses that occurred in 2020. One of the reasons for this may be that long-term historical information was incorporated into the spatio-temporal model through an autoregressive process. This spatio-temporal model was used to estimate the catch by species in the OBJ fishery for 2020 and 2021, and the results[1] indicate that the BET catch was overestimated by the BSE methodology by about 12% and 18% in 2020 and 2021, respectively, while the yellowfin tuna catch was underestimated by 18% in 2020 and overestimated by 10% in 2021; bias estimates for skipjack tuna were considerably lower. The results for 2021 are preliminary, however, because the 2021 estimates are based on data for 2020, which was also impacted by the pandemic, and possibly in a different manner than that which occurred in 2021. Further research needs to be conducted to determine the robustness of the 2021 estimates and to develop spatio-temporal models for the other set types.

2. BACKGROUND

Due to the COVID-19 pandemic, in 2020 - 2021 it was not possible to collect some of the data used to estimate the species and length composition of the tropical tuna catch (yellowfin, bigeye and skipjack) for the purse-seine fleet. Specifically, data collected in port (port-sampling data) were not collected during part of this two-year period in some of the main ports where bigeye tuna (BET) catch is unloaded (landed). As a result, there is concern that the Best Scientific Estimates (BSE) of the species and length composition of the catch for these two years may be biased, particularly for bigeye tuna (SAC-13 INF-L). The fact that the 2020 BSE of the BET catch in floating-object (OBJ) sets increased, relative to the 2019 estimate (SAC-13-03), while the number of OBJ sets in 2020 decreased relative to the number in 2019 (SAC-13-06), has added to concern about bias. Therefore, for 2020 - 2021, modification to the statistical methodology used to estimate the tropical tuna catch composition is likely necessary, placing greater emphasis on other data sources, besides the port-sampling data, in the estimation methodology.

2.1 Data sources available for catch composition estimation

There are four primary data sources available with which to estimate the species composition of the purse-seine catch of tropical tunas in the eastern Pacific Ocean (EPO): (i) Observer data, (ii) Logbook data (iii) Cannery data, and (iv) Port-sampling data. These data sources differ in their coverage, collection methods, sample sizes, potential biases (both catch amounts and species identification), and the effects of COVID on data collection. A more detailed description of these data sources is provided in Appendix C.

Of the four data sources, the observer and logbook data are the most extensive in terms of spatial and temporal coverage of the fishery. The logbook data are available for all size classes of purse-seine vessels. The logbook data include details of the fishing effort and estimates of the target species catch, but they do not provide information on the size of fish and rely on the fishers to provide information. The observer data have effectively 100% coverage for large purse seiners (IATTC Class-6; > 363 mt fish carrying-capacity) and contain additional information (e.g., bycatch, tuna discards), but are only available for a small fraction

[1] The following correction was made to the 2020-2021 CAR estimates: updated to reflect the latest total fleet catch of tropical tunas.

of small purse-seine vessels. The observer data provide estimates of the amounts of tuna catch by species in three weight categories ('small': fish < 2.5 kg total weight; 'medium': fish between 2.5 kg and 15 kg; 'large': fish > 15 kg), but not actual measurements of length or weight of individual fish.

Cannery data are principally estimated catch amounts of target species by trip, provided to the IATTC staff by tuna canneries. They do not provide information on exact fishing locations or dates, or on operational characteristics (e.g., purse-seine set type), although information on fishing zones and trip departure and arrival dates are provided. No size information is currently available on the database; some canneries do provide estimates of catch by weight categories, but those categories differ among canneries, making the size information problematic to use for catch composition estimation. Cannery data are not available to the IATTC staff for all trips nor from all canneries. The port-sampling data are collected by IATTC field office staff when purse-seine vessels unload their catch in port and are principally samples of lengths and species composition of the catch stored in individual vessel wells. The data include length measurements to the nearest mm from a sample of fish and counts of species from another independent sample of fish (see appendix in Suter (2010) for details of the sampling protocol). They also include data on the month, area and set type associated with the catch in the well that was sampled. Although the port-sampling data collection protocol is based on 13 sampling areas, since 2000 both the sampling area and the 5° area are available for each sample. Not every trip is sampled by the port-sampling program, and the coverage of trips differs by vessel size class. The coverage in terms of the percentage of wells sampled or percentage of the catch sampled is low.

2.2 Current catch composition estimation methodology

Comprehensive and accurate information on the species and size composition of the fleet catch is not available from any one of the four primary data sources. Therefore, these data sources have to be combined to produce the BSE. More information on the BSE statistical methodology used since 2000 to estimate the purse-seine tuna catch composition for the three target tuna species is provided in Appendix C and citations therein. The methodology is a design-based approach to catch estimation, as opposed to a model-based approach. The methodology uses the port-sampling data to estimate the species and size composition of the total catch of tropical tunas by stratum, where strata are defined by area and month of fishing, purse-seine set type and vessel size class category. The estimate of the total purse-seine catch of tropical tunas (sum of catches of yellowfin, bigeye and skipjack) is based on catches from cannery data, if available, otherwise observer data or logbook data are used. This total tropical tuna catch is distributed to strata using observer and logbook data.

Because there are always strata with catch but no port-sampling data (SAC-13 INF-L), species and size composition in some strata are based on port-sampling data from 'neighboring' strata. The 'best' neighboring stratum is determined through a set of hierarchical rules. In general, priority is given to set type. Then priority is given to area or month, depending on the programs being used, and finally vessel size class category. Bias may be introduced by this procedure when the true species and size composition of 'neighboring' strata with port-sampling data are sufficiently different from that of the stratum for which no port-sampling data exist. The possibility of bias is always present, but much more likely when the overall level of port-sampling is very low or catch unloaded in some ports is not sampled for an extended period of time, as was clearly the case in 2020 (SAC-13-INF-L).

2.3 Overview of statistical approach taken in this study

The overall approach taken in this study was to develop a statistical methodology that would use the port-sampling data to 'adjust,' in a statistical manner, the catch composition estimates obtained from the observer and logbook data. There are two reasons for this. First, collection of observer and logbook data was not as severely impacted by the pandemic as was the collection of port-sampling data. Second, as

noted above, the observer and logbook data are also more extensive in their spatial and temporal coverage of the fishery, as compared to the port-sampling data. Thus, the goal was to develop an integrated statistical model, which could accommodate multiple sources of variation inherent in the data, so that observer and logbook data could be used to predict the port-sampling catch composition by strata (e.g., by year and set type for specific spatial units), for strata for which no port-sampling data were actually available.

Conditionally Auto Regressive spatio-temporal models (CAR; Besag *et al.* 1991) was the class of integrated statistical models used in this study. These types of models can take advantage of innate spatial and temporal correlation structure in the data, and are thus more likely to make reliable estimates when large amounts of data are systematically missing (e.g. for certain ports for many months). The work to date has focused on estimation of the species composition of the catch in OBJ sets because BET is primarily caught in OBJ sets (SAC-13-03) and the systematic loss of port-sampling data caused by the pandemic likely led to bias in the BET OBJ-set BSE (SAC-13 INF-L).

Since the true species composition of the catch is unknown, in this study it was assumed that the goal is to develop a method that will produce catch estimates that are as consistent as possible with those produced by the BSE methodology prior to the pandemic (i.e., prior to 2020). Therefore, not only were standard measures of model performance used to develop the best CAR model, such as percent of variance explained by the model and prediction error, but the new methodology was also evaluated in terms of its ability to match the BSEs for 2000-2019 that are reported in the IATTC Fishery Status Report (e.g. Table A-7 of SAC-13-03).

In this document, we present work on a new methodology to estimate the species composition of the tropical tuna catch, focusing on OBJ sets. First, we describe the exploratory analyses used to investigate the relationship between port-sampling and observer species composition estimates. Second, we describe the new integrated statistical methodology developed to estimate the species composition of the catch from both observer (logbook) data and port-sampling data. We conclude with revised estimates of catch by species for 2020 and 2021, a retrospective evaluation of the bias if the missing data for 2020 occurred in earlier years, and a discussion about future work.

3. DATA EXPLORATORY ANALYSIS

Several types of exploratory analyses, focusing on the data of IATTC Class-6 vessels, were conducted to investigate the relationship between the species composition estimates from port-sampling and those from observer data. First, the magnitude of differences in species catch composition between observer and port-sampling data was evaluated, by strata, using graphical techniques. Then, multiple regression analyses were carried out to: (i) understand the strength and nature of the relationship between the observer and port-sampling species composition estimates; and, (ii) to identify any spatial and temporal structure that may be present in the port-sampling species composition estimates.

3.1 Graphical data summaries

To graphically explore the relationship between the port-sampling species composition proportions, p_{kt}, and the observer species composition proportions, q_{kt}, where *k* indicates the spatial unit and *t* indicates the temporal unit, the estimates from the two data sources were compared at their finest common resolution, which is a 5° area x month x year. For each data source, the species composition proportions, by stratum, were computed as the ratio of the catch of the species of interest in the stratum to the sum of the catches of all three tropical tuna species in the stratum.

If there is a simple linear relationship between the two sets of proportions for a given species, then it might be expected that

$$p_{kt} = a + b\, q_{kt} + e_{kt}$$

where *e* is the random error. From scatter plots of p_{kt} *versus* q_{kt} (Figures 1 - 2) it is clear that there is an overall increasing relationship, but also that this relationship differs by species and that there is a substantial amount of variability. While the proportions for BET and skipjack tuna (SKJ) span the full range of (0,1), the values for yellowfin tuna (YFT) tend to be concentrated closer to the origin. The variability in these scatter plots may be due to several factors including spatial effects, temporal effects, or both spatial and temporal effects.

To explore spatial differences between the two sets of proportions for each species, annual maps of the mean of differences $(p_{kt} - q_{kt})$ were computed for each 5° area, for each of the three species (Figures 3 - 4). These maps show spatial structure, as well as inter-annual fluctuations, in the mean differences. Summarizing the 5° monthly differences into longitudinal bands (Figure 5) shows that there is considerable inshore-offshore variation in the center, spread, and shape of these collections of differences. From Figure 5 it can be seen that there is: (a) significant spatial pattern – since the medians (centers) of the 5° longitudinal box-and-whisker plot summaries change as a function of longitude; and, (b) spatial variation – since the interquartile ranges and the ranges of the box-and-whisker plots change as a function of longitude. Moreover, these spatial features change annually. An additional characteristic of the port-sampling data, in comparison to the observer data, is that its spatial extent is much more limited, even when aggregated across months within a year (marked in black in Figures 3-4 are the 5° areas where port-sampling data were not available). These results suggest there is a benefit to developing statistical models that can capture these spatial features.

3.2 Regressing port-sampling species proportions on observer species proportions

For the regression analyses, the following simple model was fitted to the data of each year (the natural logarithm transformation was used because it is variance stabilizing and ensures that the estimated species proportions are between 0 and 1):

$$\log(p_{k.}) = a + b \log(q_{k.}) + e_{k.}$$

where *k* corresponds to a 5° area and the species proportions have been pooled over months of the year. The results of this regression analysis indicated that the model was a good fit to the data in that the R^2 and the $adj\ R^2$, which are indications of how well the linear regression equation explains the variation in the response variable, were in the range of 30-50%. This implies that, when data are pooled over months within a year, there is a stronger relationship between *p* and *q* than was seen in Figures 1 - 2. This is perhaps not surprising because aggregation over months leads to more data points per 5° area, and the central limit theorem asserts that the means (in this case, the proportions) should converge to the true proportions, and variances reduce significantly, as the sample size increases.

Next, with a view to improving model fit by explaining some of the spatial variation observed in Figures 3-4, latitude ("lat"), longitude ("long"), and a latitude-longitude interaction term were included in the regression model:

$$\log(p_{k.}) = a + b_1 \log(q_{k.}) + b_2 lat_{k.} + b_3\, long_{k.} + b_{23}\, lat_{k.}\, long_{k.} + e_{k.}$$

For every year, all the regressors were statistically significant for each of the three species. That is, the model fit was improved significantly by including latitude, longitude, and the latitude-longitude interaction term in the model. For example, for 2017 for BET, the results of fitting the above model are given in the following table:

Coefficients:				
	Estimate	Std Error	t-value	*p*-value
Intercept	-7.29	0.72	-9.9	< 2e-16
$\log(q_{kt})$	0.55	0.07	7.6	3.54E-13
lat_{kt}	0.29	0.05	5.1	5.30E-06
$long_{kt}$	-0.04	0.005	-8.5	1.52E-15
$lat_{kt}\ long_{kt}$	0.002	0.0005	4.7	3.22E-06

The variance explained by this regression model was 45%. The residual standard error was 1.227 on 255 degrees of freedom, and the F-statistic was 54.21 on 4 and 255 degrees of freedom, while the *p*-value for this model was 2.2e-16. By comparison, the variance explained when no spatial information was included in the model was only 29%. This is an indication that further spatial modeling would be beneficial.

4. STATISTICAL SPATIO-TEMPORAL MODELING

In this section, the CAR spatio-temporal model (Besag et a*l.* 1991) implemented in this study is described. Spatial CAR models with no temporal component were also considered in preliminary analyses but because of their poor performance, were not used for the final analysis (those models and their performance are described in Appendix A and Appendix B respectively.) This section begins with a description of the key aspects of the statistical modeling that were needed to address the data characteristics identified by the exploratory analyses. The 'best' spatio-temporal CAR model developed is then described. In the latter part of this section, the results related to model fit and prediction performance are presented, as well as estimates of the species composition of the catch, which are compared to the BSEs presented in SAC-13-03.

The key aspects of the statistical modeling that are needed to address the data characteristics are:

1. The statistical model needs to allow flexibility for spatial pattern (mean at each spatial location) and spatial variation (variance at each spatial location) in the data to change from year to year, all in one integrated model. The presence of spatial pattern implies that observations from units closer to each other are more similar than those from units farther from each other. If there is a flat spatial pattern and the spatial variance is also constant, for example, the data can be assumed to be distributed randomly in space. However, in the exploratory analyses, it was found that the BET species proportions exhibited spatial pattern and spatial variation that changed over the years. Specifically, the box-and-whisker plots of Figure 5 have different medians and different interquartile ranges, and these values depend on longitude, which suggests that there may be residual spatial pattern and spatial variation after regressing port-sampling proportions on observer proportions.
2. The statistical model needs to address data sparsity in space and time. Data sparsity is a function of the spatio-temporal resolution of the data used to fit the model. While statistical models can be fitted to relatively fine-resolution data (e.g., 5°-monthly data), the sparsity of the port-sampling data in space and time, compared to spatio-temporal extent of the catch data (observer, logbook), made such modeling of the port-sampling species proportions problematic in preliminary analyses. An example of spatial data sparsity in the monthly 5° data is shown in Figure 6. One way to address this issue is to aggregate the data in space and time to compensate for low sample sizes in certain areas of the EPO, especially in some years where data were particularly spatially scarce. However, sparsity is still present in the annual data, as shown in Figures 3 - 4. An additional

way to deal with data sparsity is to take advantage of correlation structure within the data, either in space at the same time point, or through time, by incorporating data from multiple years into one model. In this way, the model can take advantage of spatial pattern that is evolving in a correlated manner through time to help mitigate the issue of data sparsity.

3. The statistical model must be able to predict for new areal units to be able to estimate species proportions for areal units where port-sampling data were missing in 2020-2021.

After several attempts to develop models using finer-resolution data, e.g., monthly and quarterly data at a 5° spatial resolution, which resulted in models with poor performance (but see Discussion section), it was decided to aggregate the data in time to a yearly resolution and in space to the 13 sampling areas (Figure 7) used in BSE catch estimation methodology (Tomlinson 2002). The spatial aggregation works well in reducing the variability of the proportions – leading to better fitting models, presumably because there are more data points in these larger regions compared to smaller spatial 'cells'. Thus, spatio-temporal CAR models, described below, were fitted to the aggregated data to estimate p_{kt}.

4.1 Spatio-temporal CAR models for p_{kt}

Software for spatio-temporal modeling with conditional autoregressive priors using MCMC simulation was not previously available, which motivated the development of the CARBayesST package (Lee, Rushworth, and Napier 2018) in R (R Core Team 2021). The CARBayesST package was used for most analyses presented below. In all cases, inference is in a Bayesian setting using Markov Chain Monte Carlo (MCMC) simulation. In this section, the general hierarchical model that was fitted is described.

The general model formulation is given by:

$$\log(p_{kt}) = Y_{kt}$$
$$Y_{kt} \mid \mu_{kt} \sim Normal(\mu_{kt}, \nu^2)$$

$$\mu_{kt} = X^T\beta + \psi_{kt}$$

where X is a matrix of covariates and β is the regression coefficient vector. In our modeling context, $X^T\beta = a + b_1 \log(q_{kt})$, which was the first part of the multiple regression model used in the exploratory analyses described above. ψ_{kt} is the spatio-temporally autocorrelated random component (described in detail in Section 4.2) and ν^2 denotes the residual error, which is assumed to be a combination of variability around the relationship, model misspecification, and measurement error. The priors for the fixed effects parameters are given by:

$$\beta \sim N(\mu_\beta, \Sigma_\beta);$$
$$\nu^2 \sim \text{Inverse-Gamma}(a,b)$$

The hyper-parameters *a, b* can be chosen according to the problem. Usually *a, b* are chosen to make the Inverse-Gamma distribution flat (or, equivalently, to have a large variance). μ_β, Σ_β are chosen to make the Multivariate Normal distribution centered around zero with large variance.

4.2 Space-time random effects structures in the CAR model

Allowing the spatio-temporal model to take advantage of any temporal autocorrelation in the p_{kt} is an one means of compensating for sparse data, while improving model performance. To take advantage of temporal correlation within the spatio-temporal model, the temporal aspect of the spatio-temporal random effect is modelled as a first order autoregressive process (using the ST.CARar function in the CARBayesST package). Specifically, ψ_{kt} is the latent or random `spatio-temporal' variable defined on the

k[th] areal unit (in our case, one of the M = 13 sampling areas of Figure 7) and t[th] temporal unit (in our case the t[th] temporal unit will be a year, for example t = 2017). ψ_{kt} was defined as follows:

$$\psi_{kt} = \phi_{kt}$$

$$\Phi_t \mid \Phi_{t-1} \sim \mathrm{N}(\ \rho_\mathrm{T}\, \Phi_{t-1},\ \tau^2\, \boldsymbol{Q}(\boldsymbol{W}, \rho_S)^{-1}\ )$$

$$\Phi_1 \sim N(\mathbf{0},\ \tau^2\, \boldsymbol{Q}(\boldsymbol{W}, \rho_S)^{-1}\ )$$

$$\tau^2 \sim Inverse\ Gamma(c, d\ )$$

$$\rho_s, \rho_T \sim Uniform(0, 1)$$

where $\phi_t = (\phi_{1t},\ \phi_{2t}, \ldots, \phi_{NT})$ is a vector containing the spatial random effects at time t. This has a `dynamic' evolution through time via a first order autoregressive process. This evolution was assumed to have a conditional distribution of $\Phi_t \mid \Phi_{t-1}$ which is Multivariate Normal. Thus, temporal autocorrelation is induced via the mean, $\rho_\mathrm{T}\, \Phi_{t-1}$, whereas spatial autocorrelation is induced through the variance $\tau^2\, \boldsymbol{Q}(\boldsymbol{W}, \rho_S)^{-1}$. τ^2 is the spatial variance; the global spatial autocorrelation and global temporal autocorrelation coefficients are ρ_S and ρ_T respectively – hence have values in the range of -1 and 1. The hyper-parameters *c* and *d* were chosen to so as to make the Inverse-Gamma distribution flat. Several options for the order and extent (number of years) were considered for the autoregressive process. The best option is described in Section 5.1 and alternate options that were considered are discussed in Appendices A - B.

$\boldsymbol{W}$ is referred to as the neighborhood or adjacency matrix (it is symmetric), where $\boldsymbol{W} = (w_{kj})$ and w_{ik} gives the weights of the strength of the spatial association between the i[th] and k[th] regions. The only requirement is that the row totals of **W** add up to a positive value. Most often **W** is chosen to be binary, i.e., w_{kj} = 1 if the k[th] and i[th] area share physical boundaries, otherwise it is 0. $\boldsymbol{Q}$ is a function that helps to transform the *W* matrix to meet the needs of a covariance-variance matrix and it is given by

$$\boldsymbol{Q}(\boldsymbol{W}, \rho_S) = \rho_s\, [(diag\ \boldsymbol{W}.\mathbf{1}) - \boldsymbol{W}] + (1 - \rho_S\ )\boldsymbol{I}$$

Several options for the structure of the $\boldsymbol{W}$ matrix were explored in the preliminary analyses. Given that one of the goals of this study was to develop a spatio-temporal model that produced similar catch composition estimates to the BSE methodology in years prior to 2020, the final structure of $\boldsymbol{W}$ used was related to spatial aspects of the BSE methodology (See Section 5.1). Other structures explored for $\boldsymbol{W}$ in preliminary analyses are described in Appendix A.

4.3 Catch estimation

Once the estimated values for the port-sampling species proportions have been obtained, the next step is to estimate the total catch of a species for OBJ sets for the entire EPO, by year. To estimate the total catch, estimated species proportions, p_{ktm}, were obtained by spatial region (*k*), year (*t*) and vessel size class category (*m*; Classes 1-5 and Class-6). For Class 1-5 vessels, the CAR models used both observer and logbook data to compute q_{ktm}, whereas for Class-6 vessels, the q_{ktm} were based only on observer data. If the total tropical tuna catch for the EPO in year *t* is given by U_t, then U_t is prorated to area and vessel size class category using the proportion of tropical tuna catch within each stratum, as estimated from observer and logbook data. This procedure produces stratum-level estimates of total tropical tuna catch, U_{ktm}. Then the estimated catch for that stratum for a species is $U_{ktm}\, p_{ktm}$, and the total catch for OBJ sets is obtained as the sum $C_t = \sum U_{ktm}\ p_{ktm}$ over the corresponding strata. Once total catch estimates for BET and SKJ are obtained in this way, we obtain the total catch estimate for the YFT by subtracting their sum from the total OBJ catch of tropical tunas of that year. That is, $C_{t\_YFT} = U_t - C_{t\_BET} - C_{t\_SKJ}$.

5. RESULTS

5.1. Spatio-temporal modeling

a) Model parameters

Because one of the goals of the statistical modeling was to match as closely as possible the BSEs for 2010-2019, a spatial adjacency matrix ***W*** was defined that was similar to the spatial substitution rules used in the BSE estimation methodology. The spatial substitution matrix that is used in the BSE methodology (Table 1) gives, for each of the 13 areas (Figure 7), the 12 areas that should be used as substitutes, ranked by preference. In creating ***W*** for the spatio-temporal CAR model, these preferences were mimicked as closely as possible. To do this, if the kth area is the nth option as a substitute for the jth area, then $w_{jk} = w_{kj} = \nu^n$, where ν is a parameter introduced to keep the structure flexible. To maintain the rationale of the substitution rules, it was necessary to have $1 \geq \nu > 0$. The less desirable an area is as a substitute; the larger *n* is and the smaller the value of w_{jk}. Several different values of ν were tried, and from model diagnostics and prediction error diagnostic measures, a value of $\nu = 0.001$ was selected as optimal. The choice of a small value of ν implies that when $n > 1$, the ν^n will be very small, thus mimicking the low preference of some areas as substitutes (i.e., the areas in the last rows of Table 1). Finally, it is noted that the substitution rules shown in Table 1 are not always symmetric, and thus, some adjustments to the formulation above had to be made so that ***W*** would be a symmetric matrix and yet still reflect the preferred substitutions shown in Table 1. The resulting ***W*** is shown graphically in Figure 8.

With an annual time step, two options for the autoregressive process were considered: (i) a short-term model when three consecutive years were used in the model (for example, predictions for 2010 would be based on data from years 2008, 2009, and 2010): and, (ii) a long-term model where five consecutive years were used in the model (or more, as in the case of 2021). The long-term model performed better in terms of correlation with the BSE for the years 2010-2019, when the pandemic was not present. Hereafter, this long-term model will be referred to as the `best' CAR model.

The parameter estimates for the best CAR model for each year are given in Appendix B. There is some difference in the parameter estimates among years. The error variance ν^2, and spatial variances τ^2 are small, signifying that the models perform well in capturing most of the variation in the available data. The spatial correlation ρ_S and the temporal (annual) autocorrelation ρ_T are positive and moderately high; this supports the use of spatio-temporal models. Also, the intercepts and slopes of the regression function vary somewhat with vessel size class category, species, and year. So, it is reasonable to say that the relationship between the observer and port-sample species proportions varies annually for OBJ sets.

b) Catch estimates

The catch estimates of each species for OBJ sets based on the best CAR model for each of years 2010-2019 are given in Table 2, and those for 2020 and 2021 are shown separately in Table 3.

c) Model performance

The proportion of variation explained by the annual models and normalized prediction errors (squared root of the sum of squared prediction error divided by the variance of the data) indicated the models fitted the data reasonably well. The results of model performance are summarized in Tables 4 - 5. The proportion variance explained by these models ranges from 74-100%, and is mostly higher than 90%, indicating that the models fit the data well. The normalized prediction errors are mostly small (i.e., less than 1) indicating overall good prediction performance.

The results of the third measure of performance, correlation to the historical BSEs (Table A-7 in SAC-13-03), for each of the three species, are shown in Figure 9 and Table 6. If it is assumed that the BSEs for

2000-2019 are 'truth', then the new catch estimation methodology can be applied to those years and the estimates compared to the historical BSEs using the correlation coefficient (ignoring the error of the two sets of estimates). For the estimates from the best CAR models, the correlation coefficient was 0.78[2] for BET, 0.98 for SKJ and 0.95 for YFT.

d) Estimated bias

One of the main objectives of this work was to investigate the bias in the BSE due to the pandemic-driven port-sampling data loss in 2020-2021. The spatio-temporal CAR models that were developed to be consistent with BSE during non-pandemic years 2010-2019, were found to perform similarly well (see Section 5.3) when port-sampling data for some ports for which data were systematically missing in 2020 (SAC-13 INF-L) were excluded in the years prior to 2020. This robustness was taken to indicate that these best spatio-temporal CAR models would likely produce reliable estimates in 2020-2021. Given this, the bias of the BSE for a particular species was defined as the difference between the BSE estimate and the CAR estimate, divided by the CAR estimate (Table 7). The estimated bias[3] was high for BET, with 12%bias in 2020 and 18% bias in 2021 , and also high for YFT, with -18% in 2020 and 10% in 2021, and was lowest for SKJ (0.6% and -6% for 2020 and 2021, respectively).

5.2. Retrospective analysis of bias

To evaluate the effect of the pandemic-driven loss of port-sampling data on the 2020 OBJ BET BSE, the BSE estimation methodology was run for each of years 2010 - 2019, using all available cannery, observer and logbook data, but with only a subset of the port-sampling data; details of this analysis can be found in SAC-13 INF-L. The results indicate that the systematic pandemic-related loss of port-sampling data in 2020 for ports where much of the EPO BET is estimated to be unloaded may have led to a bias in the OBJ BET BSE. Although the median difference between estimates, with and without the simulated data loss, was close to 0, both negative and positive biases of about 20% or more were seen over the 2010 – 2019 period (Figures 10-11). A similar analysis for 2021 has not yet been completed.

To further evaluate bias, the estimated ratios of BSE OBJ estimates divided by the best spatio-temporal CAR model estimates for three species of tuna, for the years 2020-2021, are given in Table 8. Comparing these ratios to results from the simulation study of SAC-13 INF-L (the box-and-whisker plots shown here in Figure 11), it can be seen that the ratios are close to or within the inter-quartile range of the ratios of BSE estimates, without and with the simulated pandemic data loss, obtained from that simulation study. This indicates that there is consistency between the two studies as regards the potential magnitude of the bias.

5.3. Sensitivity analysis of the best CAR model in 2020

To test the sensitivity of the CAR methodology to a systematic loss of port-sampling data in the year for which estimates were desired, a sensitivity analysis with data from 2019 and earlier was conducted, mimicking the 2020 data loss in the year of interest. Specifically, the port-sampling data from the ports of Manta (April-December), Mazatlan (April) and Posorja (April-May) (see SAC-13 INF-L for an explanation of why these ports and time periods were selected) were excluded for the year of interest and the catch totals for that year re-estimated using the same best CAR model. This was done for each of years 2010 – 2019. Comparison of these estimates to the BSEs, and to the CAR estimates based on the full data sets for

[2] The following correction was made to the CAR estimates: updated to reflect the latest total fleet catch of tropical tunas.

[3] The following correction was made to the 2020-2021 CAR estimates: updated to reflect the latest total fleet catch of tropical tunas.

2010- 2019, demonstrates that even after excluding some of the port-sampling data, the CAR estimates seem robust, since they are close to the estimates obtained when the data were not excluded (Figure 12).

To further demonstrate the robustness of the CAR estimates, Table 9 shows the correlation coefficients of the CAR estimates for the best model with the BSE (i) when no port-sampling data were excluded, and (ii) when some port-sampling data were excluded. The correlation coefficients are very similar for both (i) and (ii).

6. DISCUSSION

To address the systematic loss of port-sampling data from some ports during 2020 - 2021, a lognormal spatio-temporal CAR model was developed to obtain annual estimates of the species composition of the catch in OBJ sets. This modeling approach makes use of the observer (logbook) data, as well as the spatial and temporal structure inherent in the available port-sampling data, to predict the species catch composition for estimation strata for which no port-sampling data were collected. The spatial correlation structure of the CAR model was specifically designed to mimic the spatial dependencies inherent in the current BSE methodology. Thus, this CAR model can be viewed as an extension of the current BSE methodology, one which can take advantage of other data sources to mitigate the normal sparseness of the port-sampling data – a feature exacerbated by the effect of the pandemic on data collection in 2020 - 2021. This CAR model was shown to have good performance in terms of percent variation explained and normalized prediction error, and the annual estimates produced by the CAR model had reasonably high correlation with the 2010-2019 BSEs for OBJ sets. In addition, the estimates of the CAR model were reasonably consistent with the BSE estimates even when trips were excluded systematically in the years prior to 2020 to simulate the pandemic-driven data loss. One of the reasons for this may be that the CAR model incorporated long-term historical information in a structured manner, which may be a reliable method to correct for short-term systematic data loss.

The CAR model was used to estimate the potential 'bias' in the BSE for OBJ sets for 2020 and 2021, for each of the three tropical tuna species. From these results[4] it seems that the BET catch may have been over-estimated by the BSE methodology for the years 2020 and 2021 by 12 and 18%, respectively. The percent bias for BET in 2021 (18%) and YFT in 2020 (-18%) was greater than the differences between the BSE and the CAR estimates in 2010-2019, years for which no bias in the BSE would be expected because there was no systematic loss of port-sampling data. In contrast, the 'bias' values for SKJ for 2020 and 2021 were within the range of values obtained for the earlier years, i.e., 2010 - 2019. This suggests that, of the three species' estimates for 2020 – 2021, those for SKJ were the least likely to have been impacted by pandemic-related data loss.

The pandemic appears to have had less of an impact on the fishery and sampling in 2021, as compared to 2020. The number of OBJ sets and fishing capacity increased compared to 2020 (SAC-13-06) as did the number of wells sampled by the port sampling (there were 447 well samples used in the analysis for 2020 and 611 for 2021). However, despite the increase in fishing effort, the BSE estimate of bigeye tuna catch decreased (SAC-13-06). In addition, the estimated bias in the BSE estimates for BET were about the same as in 2020 and 2021, despite the increase in wells sampled by the port-sampling program. There may be several reasons for these unexpected changes. The retrospective analysis of the BSE catch estimates showed that there may be bias in the BSE estimates in the case of systematic data loss, but there could be both over and under estimation of catch in different years. In addition, the time series nature of the CAR estimator means that the 2020 port-sampling data, which had significant data gaps for some ports, were used in the estimation of the 2021 catch composition (although, to compensate for this a longer

[4] The following correction was made to the 2020-2021 CAR estimates: updated to reflect the latest total fleet catch of tropical tunas.

time series was used). Other factors such as bigeye tuna abundance could also impact the estimates. Therefore, further work is needed to investigate the reliability of the 2021 catch and bias estimates. In particular, we plan to conduct a full sensitivity analysis for 2021, as was done for 2020. This is important because the effect of the pandemic on 2021 port-sampling data availability may be different than was seen in 2020, and this could have implications for the formulation of the AR process in the CAR model, especially given the spatio-temporal movements of the fleet within the EPO over the course of a year.

7. FUTURE WORK AND DIRECTIONS

The exploratory analyses that were conducted for the unassociated sets (NOA) and dolphin-associated sets (DEL) showed that the species composition proportions, by strata, were closer to 0's or 1's (in case of DEL sets) and are sparse (in the case of NOA sets) than for OBJ sets, as reflected in Figures 1-2. Despite this, initial model fitting for NOA sets indicated that similar CAR methodology could still be used with those data, and thus this will be a topic of future research.

Building on the CAR methodology developed for OBJ sets, a next step may be to investigate estimation of the length composition of the catch of each species within the same framework to determine whether similar lognormal spatio-temporal CAR models are well-suited to those data. One challenge is that for the observer data, the available size information is ordered categories of weight (i.e., small/medium/large) rather than lengths. This may lead to aggregation of the port-sampling data into three categories of length, and eventually a categorical data analysis and consequent spatio-temporal model development.

In the future it is also of interest to determine whether fine-scale models (e.g., 5° - month or 5°- quarter) could be developed to fit the species composition data. This could be advantageous because the stock assessment models have a quarterly time step and the fisheries definitions differ from the 13 areas used in this analysis. As mentioned previously, aggregating the data to the 13 sampling areas (Figure 7) and year led to well-performing models that were also consistent with the BSE for 2010-2019. At a finer scale, there are many spatial 'cells' where port-sampling data are not available, as illustrated in Figure 6, which complicates model development. Figures 1-2 also illustrate that in the fine-scale situation, there is also the modeling challenge of dealing with many zero-valued 'observations,' and this may require the use of zero-inflated or other mixed models.

One of our priorities for this work was to come up with well-performing statistical models that could match the estimates for BSE in the years 2010-2019 and perform robustly even when data were missing systematically. However, going forward methodologies based on alternate formulations of the $\boldsymbol{W}$ (adjacency) matrix for the spatio-temporal CAR models will be considered, which may lead to alternative modeling options for estimating species composition. For instance, in Appendix A, we discuss preliminary statistical modeling efforts where different adjacency matrices were considered and performance measures for those alternate models are shown in Appendix B. We note that the performance of these models is good, yet they were not selected since they failed the 'consistency test' with respect to the historical BSE estimates for 2010 - 2019. Therefore, future work may include an investigation of alternate $\boldsymbol{W}$ matrices, where the modeling selection criteria are not constrained to include the requirement of a high correlation with the historical BSEs.

8. CONCLUSION

- The COVID-19 pandemic limited the ability of port samplers to take samples, resulting in a reduction in OBJ-set samples for 2020 and 2021 of 66% and 35%, respectively, compared to 2019.
- The port sampling data are used to calculate the species and size composition of the catch, and therefore play a very important role in the current BSE catch estimation methodology.

- Port-sampling data collection was disrupted by the pandemic in some ports more than others and this may result in bias in the estimates of catch by species because certain fleet segments preferentially unload in specific ports.
- Applying the same systematic reduction in sampling by port to the data of years prior to 2020 showed that bias could occur, but that the bias could be either an over-estimation or an under-estimation (SAC-13 INF-L).
- Exploratory analysis showed that observer data (supplemented with logbook data, where necessary) could be used successfully to predict the port-sampling species composition, and that prediction was improved when spatial and temporal covariates were included in the model.
- A spatio-temporal model was developed to estimate the port-sampling species proportions from observer (logbook) data in catch estimation strata for which port-sampling data were not available.
- Using the spatio-temporal model to estimate the catch composition of earlier years (2010-2019), after simulating the same systematic reduction in port-sampling data that occurred in 2020, showed that the catch composition estimates from the spatio-temporal model were robust to systematic port-sampling data loss for the year for which catch estimates were desired, as long as complete data were available for earlier years.
- The spatio-temporal model was used to estimate the catch by species in the OBJ fishery for 2020 and 2021, and the results[5] indicated that the BET catch was overestimated by about 12% in 2020 and by 18% in 2021.
- The results for 2021 are preliminary, however, because the 2021 estimates are based on data for 2020, which was also impacted by the pandemic, and possibly in a different manner than occurred in 2021.
- Further research needs to be conducted to determine the robustness of the 2021 estimates and to provide estimates for the other set types.

9. REFERENCES

Besag J, York J, Mollié A (1991). "Bayesian Image Restoration with Two Applications in Spatial Statistics." *Annals of the Institute of Statistics and Mathematics*, **43**, 1–59.

Lee D, Mitchell R (2012). "Boundary Detection in Disease Mapping Studies." *Biostatistics*, **13**, 415–426

Lee D, Rushworth A, Napier G (2018). "Spatio-Temporal Areal Unit Modeling in R with Conditional Autoregressive Priors Using the CARBayesST Package." *Journal of Statistical Software, Articles*, **84**(9), 1–39. Doi:10.18637/jss.v084.i09.

Lee D, Sarran C (2015). "Controlling for unmeasured confounding and spatial misalignment in long-term air pollution and health studies." *Environmetrics*, **26**, 477–487.

[5] The following correction was made to the 2020-2021 CAR estimates: updated to reflect the latest total fleet catch of tropical tunas.

Leroux B, Lei X, Breslow N (2000). “Estimation of Disease Rates in Small Areas: A New Mixed Model for Spatial Dependence.” In M Halloran, D Berry (eds.), *Statistical Models in Epidemiology, the Environment and Clinical Trials*, pp. 179–191. Springer-Verlag, New York.

R Core Team 2021. R: A language and environment for statistical computing. R Foundation for Statistical Computing, Vienna, Austria. URL https://www.R-project.org/.

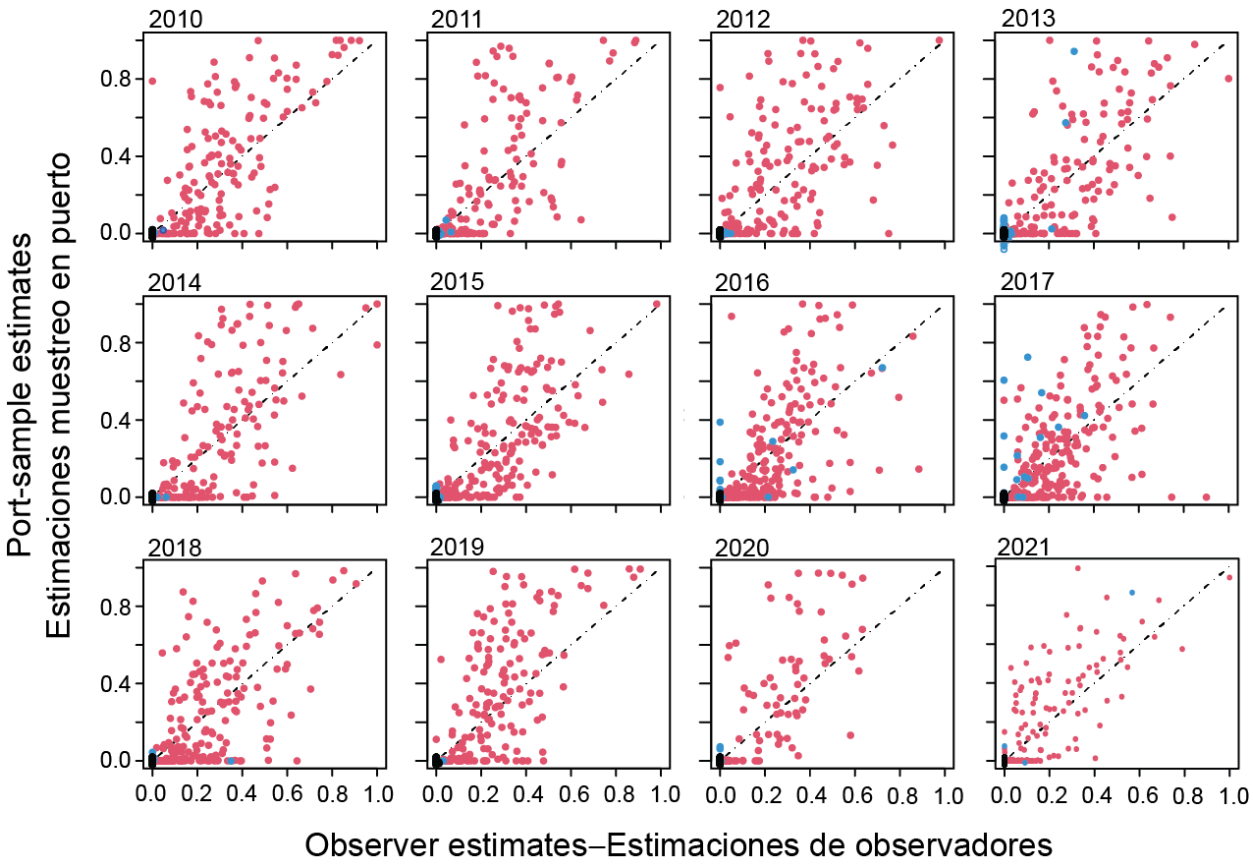

FIGURE 1. Scatter plots of the observer versus the port-sampling proportions for BET at a resolution of 5°area x month, for 2010 – 2021, plotted for `cells' that had both port-sampling and observer data. Red dots: OBJ sets; black dots: NOA sets; and blue dots: DEL sets.

FIGURA 1. Diagramas de dispersión de las proporciones de observadores frente a las proporciones de muestreo en puerto para BET en una resolución de área de 5° por mes, para 2010–2021, trazados para "celdas" que tenían datos de muestreo en puerto y de observadores. Puntos rojos: lances OBJ; puntos negros: lances NOA; puntos azules: lances DEL.

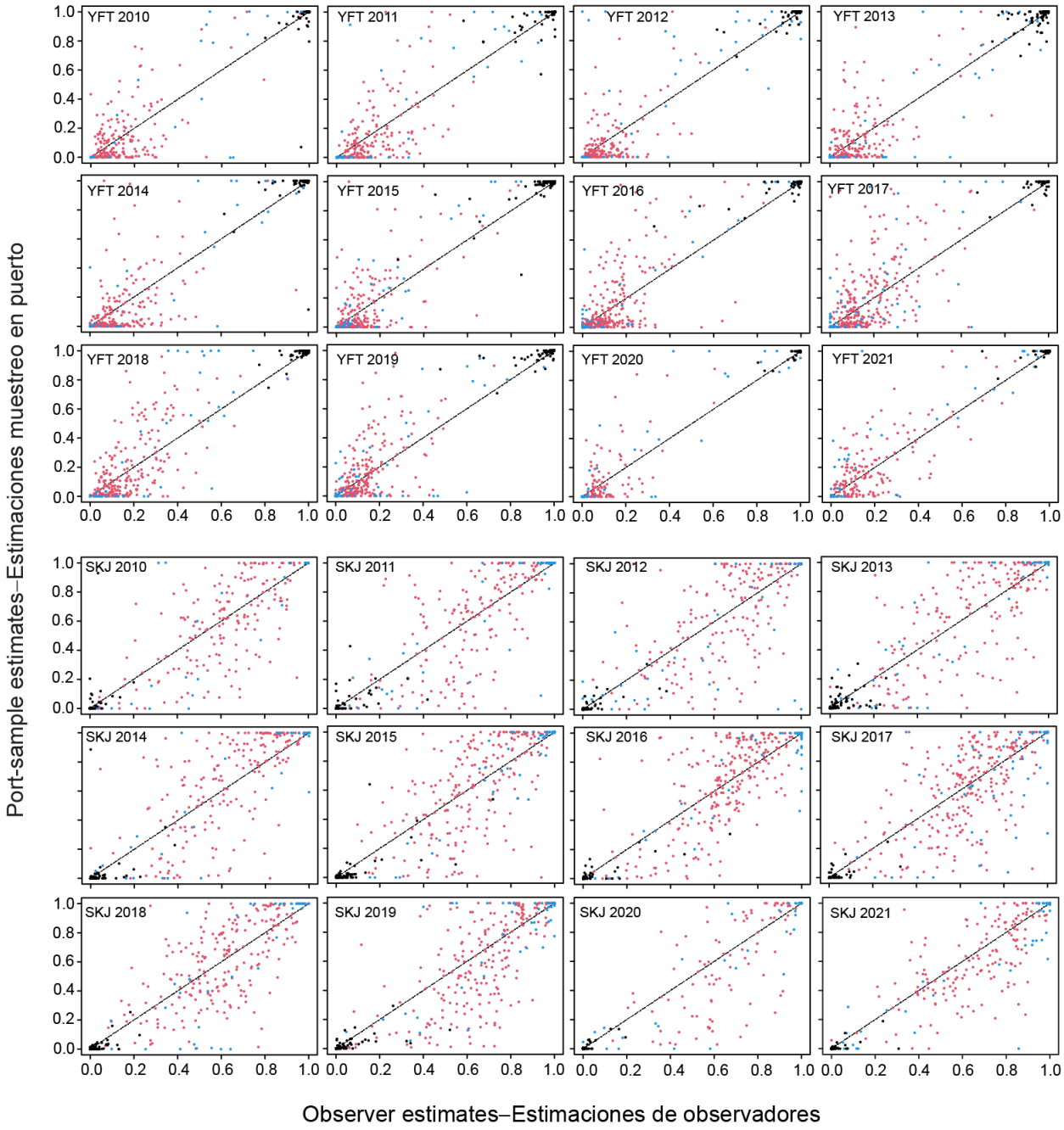

FIGURE 2. Scatter plots of the observer versus port-sampling proportions for YFT (upper panel) and SKJ (lower panel) at a resolution of 5°area x month, for 2010 – 2021, plotted for `cells' that had both port-sampling and observer data. Red dots: OBJ sets; black dots: NOA sets; and blue dots: DEL sets.

FIGURA 2. Diagramas de dispersión de las proporciones de observadores frente a las proporciones de muestreo en puerto para YFT (panel superior) y SKJ (panel inferior) en una resolución de área de 5° por mes, para 2010–2021, trazados para "celdas" que tenían datos de muestreo en puerto y de observadores. Puntos rojo: lances OBJ; puntos negros: lances NOA; puntos azules: lances DEL.

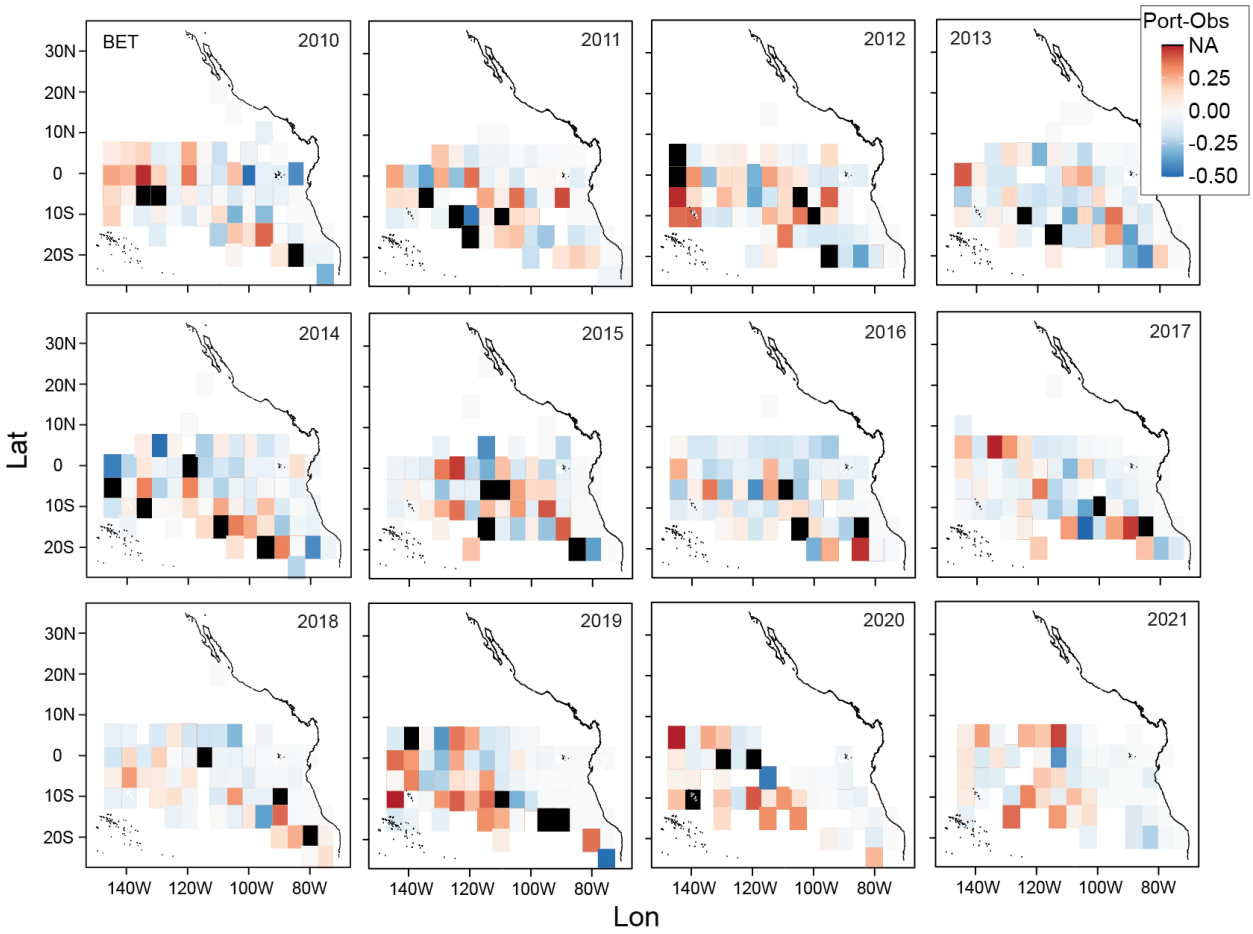

FIGURE 3. Annual maps of differences between port-sampling and observer proportions $(p_{kt} - q_{kt})$ for BET (Class-6 OBJ), at a 5° resolution. The black color indicates 5° areas for which port-sampling data were unavailable.

FIGURA 3. Mapas anuales de las diferencias entre las proporciones de muestreo en puerto y las proporciones de observadores $(p_{kt} - q_{kt})$ para BET (OBJ clase 6), en una resolución de 5°. El color negro indica áreas de 5° para las que no se disponía de datos de muestreo en puerto.

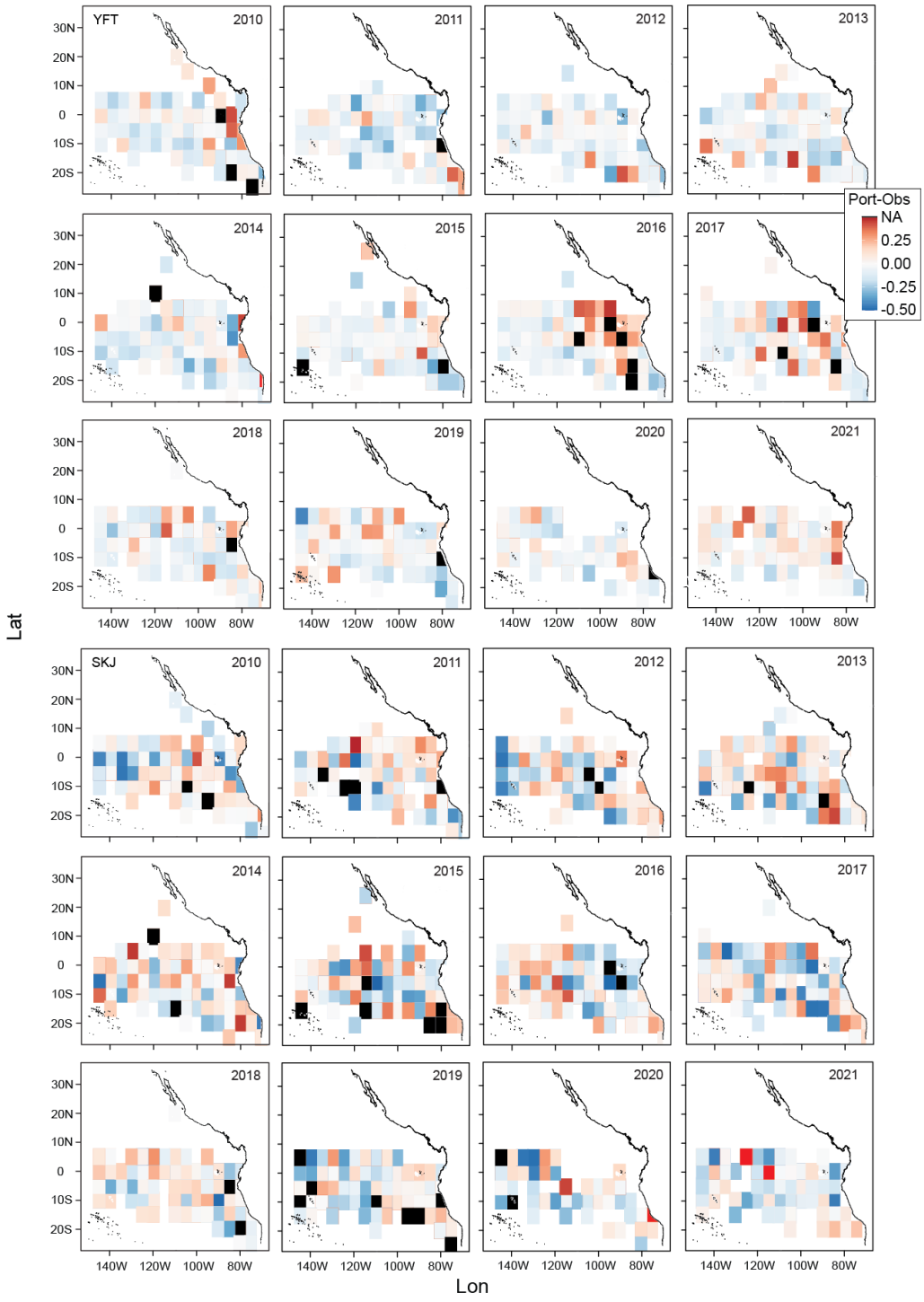

FIGURE 4. Annual maps of differences between port-sampling and observer proportions $(p_{kt} - q_{kt})$ for YFT (top panel) and SKJ (bottom panel) (both Class-6 OBJ), at a 5° resolution. The black color indicates 5° areas for which port-sampling data were unavailable.

FIGURA 4. Mapas anuales de las diferencias entre las proporciones de muestreo en puerto y las proporciones de observadores $(p_{kt} - q_{kt})$ para YFT (panel superior) y SKJ (panel inferior) (ambos OBJ clase 6), en una resolución de 5°. El color negro indica áreas de 5° para las que no se disponía de datos de muestreo en puerto.

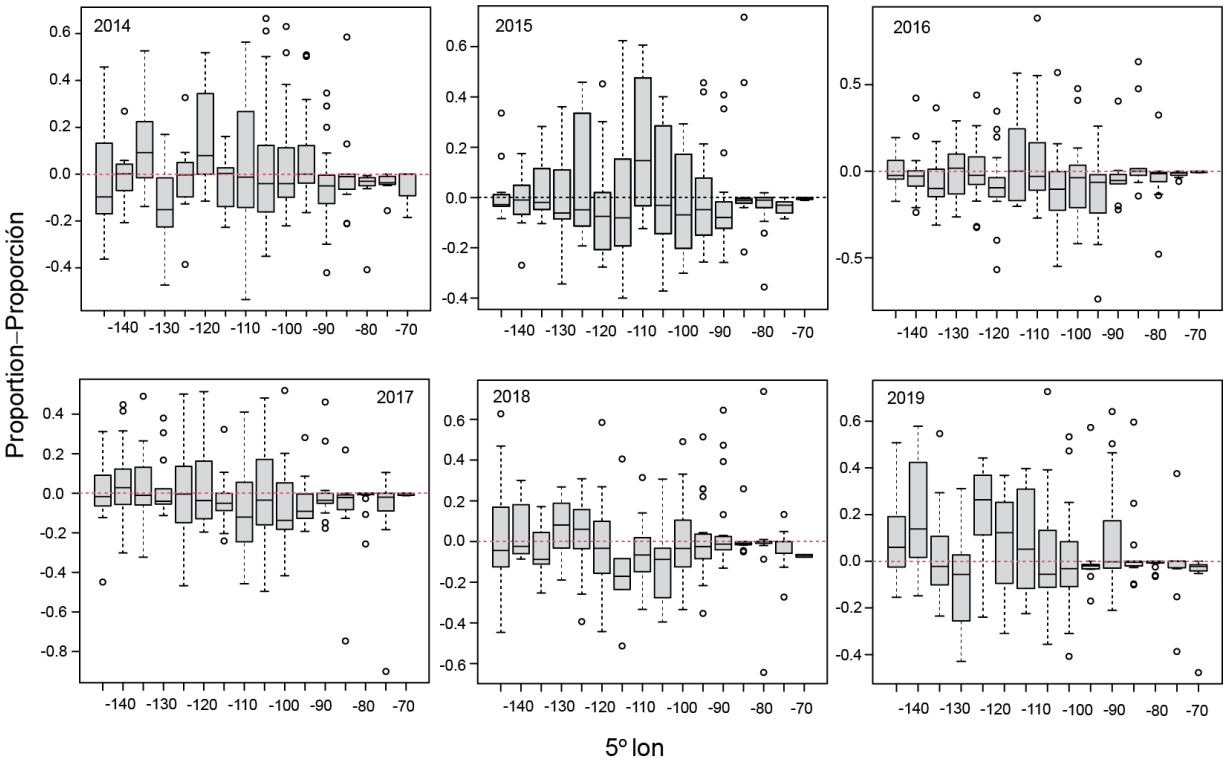

FIGURE 5. Box-and-whisker plots of the 5° x month differences between port-sampling and observer proportions of BET shown in Figure 3, for 2014-2019, grouped into longitudinal bins of 5° resolution. The horizontal bar within each gray box indicates the median difference for the 5° longitudinal bin, the gray box shows the interquartile range (the middle 50% of the values), the whiskers indicate variability outside the upper and lower quartiles, and the open circles indicate values beyond 1.5 x the interquartile range.
FIGURA 5. Gráficas de caja y bigote de las diferencias de 5° por mes entre las proporciones de muestreo en puerto y las proporciones de observadores de BET mostradas en la Figura 3, para 2014-2019, agrupadas en intervalos longitudinales de 5° de resolución. La barra horizontal dentro de cada caja gris indica la diferencia mediana para el intervalo longitudinal de 5°; la caja gris muestra el rango intercuartil (el 50% de los valores); los bigotes indican variabilidad fuera de los cuartiles superiores e inferiores; los círculos abiertos indican valores más allá de 1.5 por el rango intercuartil.

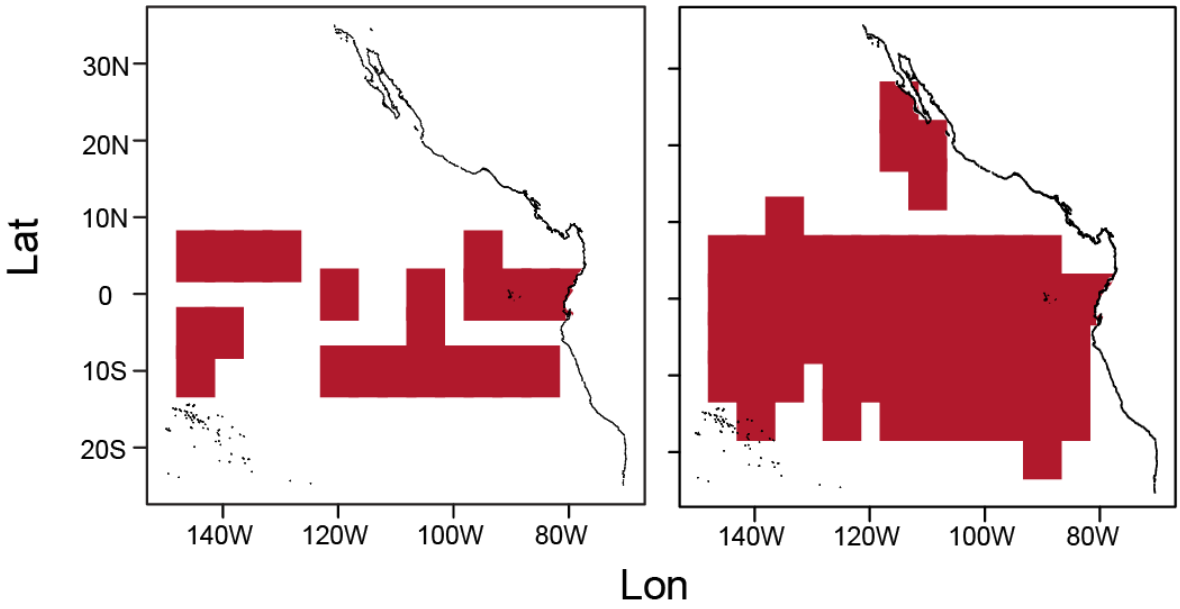

FIGURE 6. An example of the spatial sparsity of the port-sampling data, as compared to the observer data, for Class-6 OBJ, July 2017. The 5° areas shown in red denote positive catch of any of the tropical tuna species, for port-sampling samples (left panel) and observer data (right panel).

FIGURA 6. Un ejemplo de la escasez espacial de los datos de muestreo en puerto en comparación con los datos de observadores para la clase 6 OBJ, julio de 2017. Las áreas de 5° señaladas en rojo denotan capturas positivas de cualquiera de las especies de atunes tropicales, para muestras de muestreo en puerto (panel izquierdo) y datos de observadores (panel derecho).

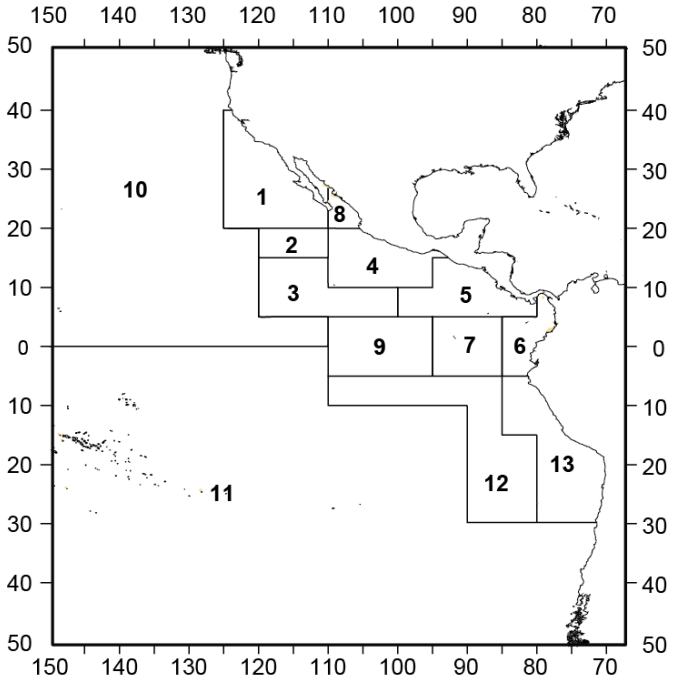

FIGURE 7. The 13 sampling areas in the EPO used for carrying out final analysis of the catch estimation (Tomlinson, 2002).

FIGURA 7. Las 13 áreas de muestreo en el OPO utilizadas para realizar el análisis final de la estimación de la captura (Tomlinson, 2002).

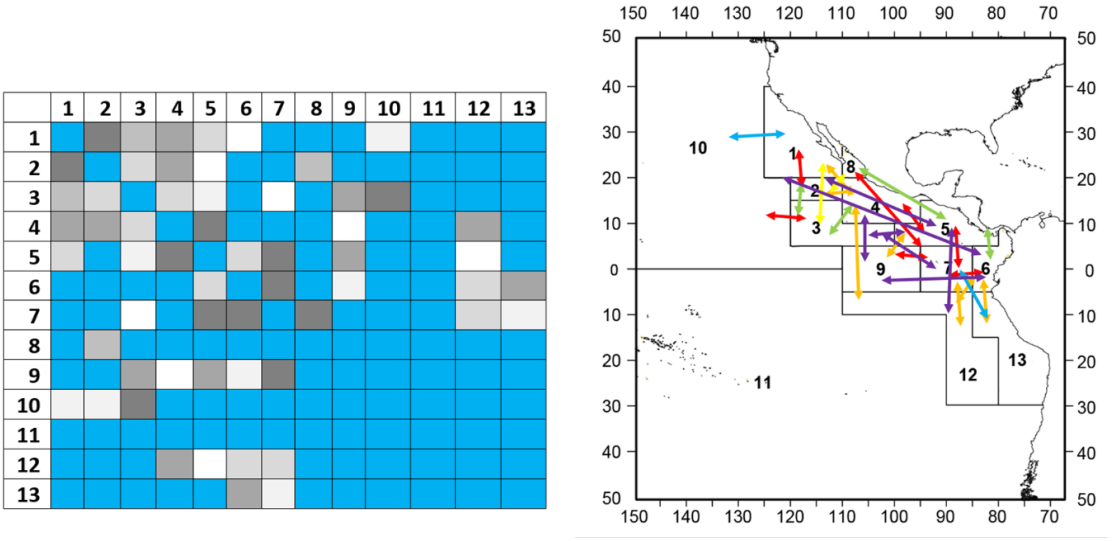

FIGURE 8. ***W*** matrix used in spatio-temporal CAR model represented as a matrix (left panel) and through arrows (right panel). In the left panel, the blue colors denote a value of zero for w_{kj} or no direct substitution. The white and black are shades to denote positive values between 0 and 1, the darker the shade, the larger the value. So, for instance for substituting for area 1, area 2 is the first choice and so on. In the right panel, the substitution rules are represented by colored arrows, with the rainbow color scheme. The substitution rules in order of the colors are red, orange, yellow, green, blue and violet. Thus, the red denotes the first order (strongest) substitution rule where the violet denotes the 6th order (weakest) substitution rule we have used.

FIGURA 8. La matriz ***W*** utilizada en el modelo CAR espaciotemporal representada como una matriz (panel izquierdo) y mediante flechas (panel derecho). En el panel izquierdo, el color azul indica un valor de cero para w_{kj} o ninguna sustitución directa. Los tonos de grises señalan valores positivos entre 0 y 1; cuanto más oscuro es el tono, mayor es el valor. Por lo tanto, por ejemplo, para sustituir el área 1, el área 2 es la primera opción y así sucesivamente. En el panel derecho, las reglas de sustitución están representadas por flechas de colores del arcoíris. Las reglas de sustitución en el orden de los colores son rojo, naranja, amarillo, verde, azul y violeta. Así, el rojo denota la regla de sustitución de primer orden (la más fuerte) mientras que el color violeta denota la regla de sustitución de sexto orden (la más débil) que utilizamos.

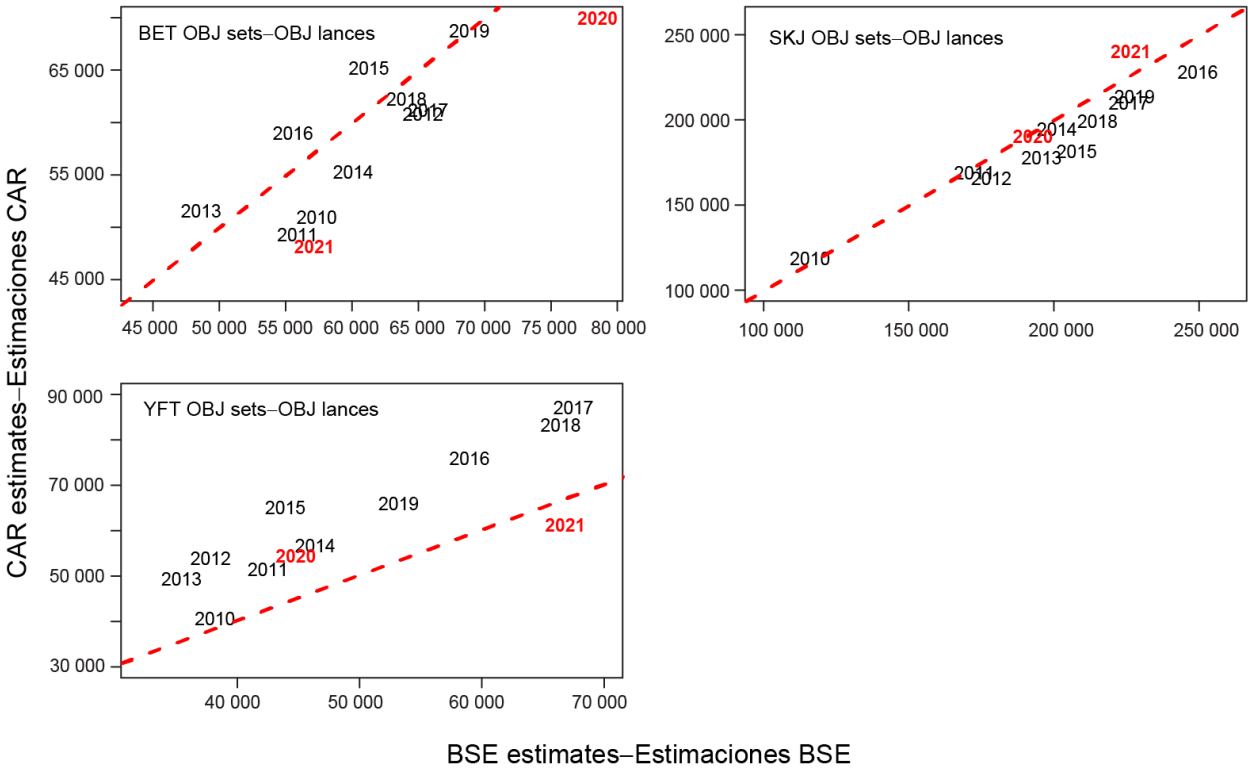

FIGURE 9. The BSE (on the x-axis) *versus* the estimates from the 'best' CAR model for 2010-2021 (y-axis), with 2020-2021 estimates shown in red, for: (a) BET (upper left panel); (b) SKJ (upper right panel); and (c) YFT (lower left panel). The following correction was made to the CAR estimates: updated to reflect the latest total fleet catch of tropical tunas.

FIGURA 9. La BSE (en el eje 'x') *versus* las estimaciones del "mejor" modelo CAR para 2010-2021 (eje 'y'); las estimaciones de 2020-2021 se muestran en rojo para: (a) BET (panel superior izquierdo); (b) SKJ (panel superior derecho); y (c) YFT (panel inferior izquierdo). Se realizó la siguiente corrección en las estimaciones CAR: se actualizaron para reflejar la captura total más reciente de la flota de atunes tropicales.

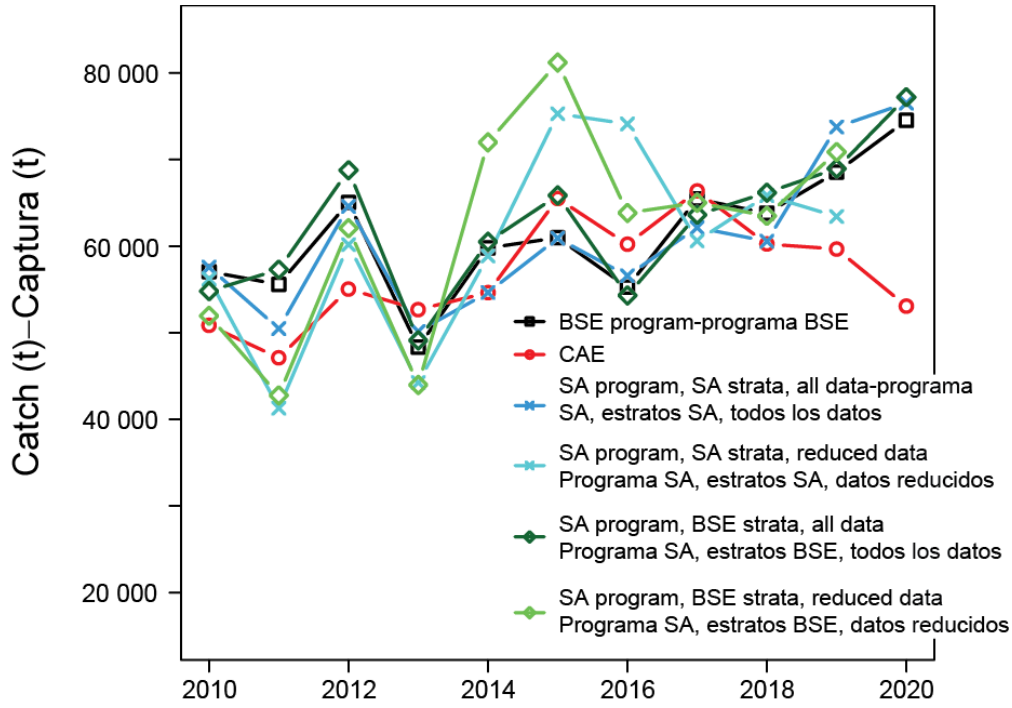

FIGURE 10. BET OBJ catch estimates for years 2010-2020. "BSE program": BSEs shown in Table A-7 of the IATTC Fishery Status Report; "SA program, BSE strata": BSEs from the stock assessment ("SA") estimation program using the BSE strata; CAE: IATTC Catch and Effort database summary (not adjusted for coverage); "SA program, SA strata": BSEs from the SA program using the SA strata; "reduced data": the estimation program used the reduced port-sampling data set (see SAC-13-INF-L for details).

FIGURA 10: Estimaciones de captura de BET en lances OBJ para el periodo 2010-2020. "Programa BSE": las BSE presentadas en la Tabla A-7 del *Informe de la situación de la pesquería de la CIAT*; "Programa SA, estratos BSE": las BSE del programa SA utilizando los estratos BSE; CAE: resumen de la base de datos de captura y esfuerzo de la CIAT (no ajustado por la cobertura); "Programa SA, estratos SA": las BSE del programa SA utilizando los estratos SA; "Datos reducidos": el programa utilizó el conjunto de datos de muestreo en puerto reducidos (ver SAC-13-INF-L para más detalles).

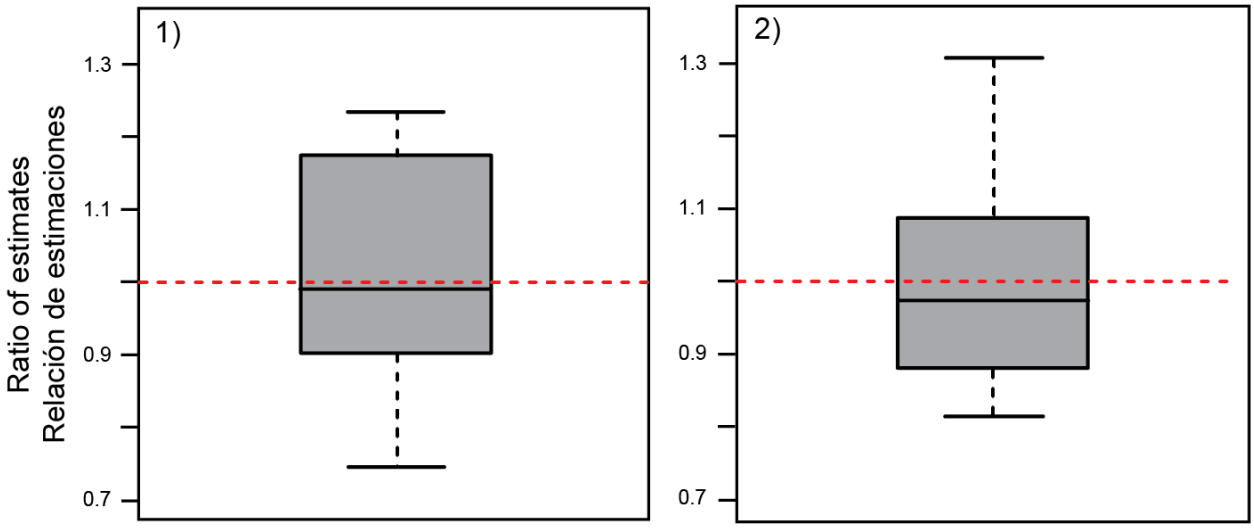

FIGURE 11. Box-and-whisker plots of ratios of some of the BET OBJ estimates shown in Figure 10, 2010 - 2019: 1) ratio of the dark green time series of Figure 10 to the light green times series of Figure 10; and, 2) ratio of the dark blue time series of Figure 10 to the light blue time series of figure 10 (see SAC-13-INF-L for details).

FIGURA 11. Gráficas de caja y bigote de las razones de algunas de las estimaciones de captura de BET en lances OBJ mostradas en la Figura 10, 2010-2019: 1) razón de la serie de tiempo color verde oscuro de la Figura 10 a la serie de tiempo color verde claro de la Figura 10; y, 2) razón de la serie de tiempo color azul oscuro de la Figura 10 a la serie de tiempo color azul claro de la Figura 10 (ver SAC-13-INF-L para más detalles).

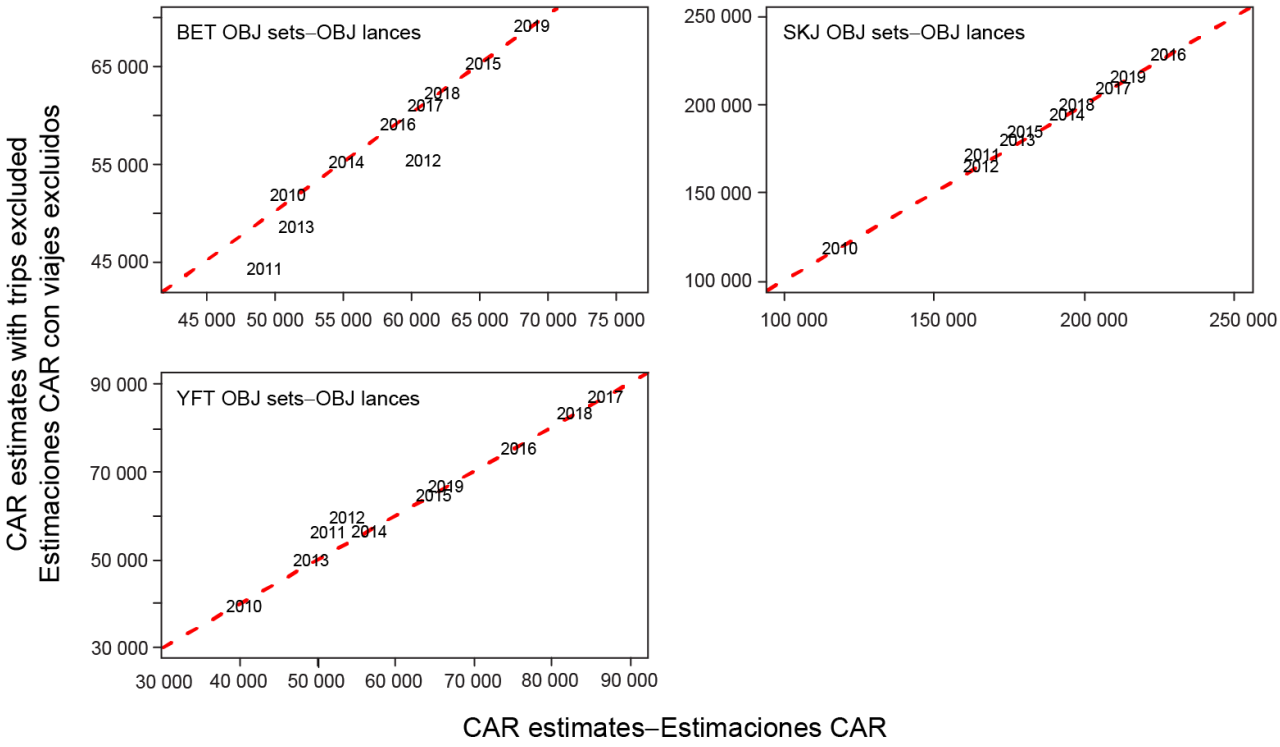

FIGURE 12. The CAR estimates with some port-sampling data excluded (on the x-axis) *versus* the CAR estimates for 2010-2019 with no data excluded: (a) BET (upper left panel); (b) SKJ (upper right panel); and, (c) YFT (lower left panel). The following correction was made to the CAR estimates: updated to reflect the latest total fleet catch of tropical tunas.

FIGURA 12. Las estimaciones CAR con algunos datos de muestreo en puerto excluidos (en el eje 'x') *versus* las estimaciones CAR para 2010-2019 sin datos excluidos: (a) BET (panel superior izquierdo); (b) SKJ (panel superior derecho); y, (c) YFT (panel inferior izquierdo). Se realizó la siguiente corrección en las estimaciones CAR: se actualizaron para reflejar la captura total más reciente de la flota de atunes tropicales.

TABLE 1. Matrix showing the area substitution choices that are used by the current BSE methodology. The top row (bold numbers, gray highlighting) gives the number of the sampling area (Figure 7) for which a substitute area is needed. The subsequent rows give the areas to be used as substitutes, starting with the preferred choice in the second row of the table, down to the least desirable choice in the last row of the table. For example, for Area 1, the best substitute is Area 8, the second-best substitute is Area 2, and so on, down to the least desirable substitute, which is Area 11.

TABLA 1. Matriz que muestra las opciones de sustitución de área utilizadas por la actual metodología BSE. La fila superior (números en negrita, resaltada en gris) proporciona el número del área de muestreo (Figura 7) para la que se necesita un área sustituta. Las filas siguientes proporcionan las áreas a utilizarse como sustitutas, comenzando por la opción preferida en la segunda fila de la tabla, hasta la opción menos deseable en la última fila. Por ejemplo, para el Área 1, la mejor sustitución es el Área 8, la segunda mejor el Área 2, y así sucesivamente hasta el área sustituta menos deseable, que es el Área 11.

1	**2**	**3**	**4**	**5**	**6**	**7**	**8**	**9**	**10**	**11**	**12**	**13**
8	1	10	5	7	7	9	1	7	3	12	13	12
2	4	9	8	9	13	6	4	3	11	9	11	6
4	8	2	3	3	5	5	2	11	2	10	9	7
3	3	4	2	6	12	12	5	12	9	7	7	9
5	10	5	1	4	9	13	3	10	5	3	6	5
10	5	7	9	12	4	3	6	5	7	5	5	4
6	9	1	10	2	3	11	7	2	1	13	3	11
7	7	12	7	10	8	4	13	4	4	6	10	3
13	12	11	6	8	2	10	9	6	12	2	2	8
12	11	6	13	1	1	2	10	13	6	4	4	2
9	6	8	12	11	10	1	12	1	8	1	1	1
11	13	13	11	13	11	8	11	8	13	8	8	10

TABLE 2. OBJ catch estimates of BET, YFT, SKJ (metric tons) for 2010-2019 based on the `best' CAR model. The BSE values were taken from Table A-7 of SAC-13-03. The following correction was made to the CAR estimates: updated to reflect the latest total fleet catch of tropical tunas.
TABLA 2. Estimaciones de captura de BET, YFT, SKJ en lances OBJ (toneladas métricas) para 2010-2019 basadas en el 'mejor' modelo CAR. Los valores BSE se tomaron de la Tabla A-7 del documento SAC-13-03. Se realizó la siguiente corrección en las estimaciones CAR: se actualizaron para reflejar la captura total más reciente de la flota de atunes tropicales.

Estimates	2010	2011	2012	2013	2014	2015	2016	2017	2018	2019
BET CAR	50909	49212.8	60780	51531	55197	65169	58943	60953	62173.9	68715
BET BSE	57059	55587	65035	48337	59797	60975	55269	65443	63815	68553
YFT CAR	40231	51011.6	53457	48828	56311	64603	75507	86681	82712.5	65568
YFT BSE	37850	42176	37487	35112	46049	43603	58673	67167	66122	52862
SKJ CAR	118427	168732	165340	177462	194034	181321	227682	209398	198677	213507
SKJ BSE	114659	171193	177055	194372	199696	206515	248190	224422	213626	226375

TABLE 3. OBJ catch estimates of BET, YFT, SKJ (metric tons) for 2020-2021 based on the `best' CAR model. The BSE values were taken from Table A-7 of SAC-13-03. The following correction was made to the 2020-2021 CAR estimates: updated to reflect the latest total fleet catch of tropical tunas.
TABLA 3. Estimaciones de captura de BET, YFT, SKJ en lances OBJ (toneladas métricas) para 2020-2021 basadas en el 'mejor' modelo CAR. Los valores BSE se tomaron de la Tabla A-7 del documento SAC-13-03. Se realizó la siguiente corrección en las estimaciones CAR de 2020-2021: se actualizaron para reflejar la captura total más reciente de la flota de atunes tropicales.

Estimated values	2020 CAR	2020 BSE	2021 CAR	2021 BSE
BET	69,901	78,208	48,088	56,861
SKJ	190,243	191,399	239,692	225,132
YFT	53,924	44,461	60,701	66,488

TABLE 4. Proportion of variance explained, and normalized prediction error (sum of prediction error divided by variance of response) for the BET and SKJ 'best' CAR models for 2010-2021, for Class-6 vessel data (OBJ sets). The values in the table are interpreted as follows: 1 is highest and signifies perfect fit while 0 is the lowest value and signifies ineffective model fitting.

TABLA 4. Proporción de varianza explicada y error de predicción normalizado (suma del error de predicción dividido por la varianza de respuesta) para los 'mejores' modelos CAR para BET y SKJ para 2010-2021, para datos de buques de clase 6 (lances OBJ). Los valores en la tabla se interpretan de la siguiente manera: 1 es el más alto y significa un ajuste perfecto mientras que 0 es el valor más bajo y significa un ajuste ineficaz del modelo.

Vessel size class 6	2010	2011	2012	2013	2014	2015	2016	2017	2018	2019	2020	2021
BET												
proportion of variance explained	0.99	0.99	0.99	0.96	0.96	0.96	1	1	1	1	0.99	0.99
normalized prediction error	0.2	0.12	0.25	0.45	0.72	0.91	0.15	0.2	0.12	0.12	0.14	0.19
SKJ												
proportion of variance explained	0.88	0.87	0.74	0.82	0.8	0.82	0.74	0.83	0.83	0.85	0.88	1
normalized prediction error	1.6	0.61	3.2	1.39	0.73	0.96	2.2	0.91	0.96	0.59	0.62	0.19

TABLE 5. Proportion of variance explained, and normalized prediction error (sum of prediction error divided by variance of response) for the BET and SKJ 'best' CAR models for 2010-2021, for Classes 1-5 vessel data (OBJ sets). Values smaller than 1 indicate good prediction performance.

TABLA 5. Proporción de varianza explicada y error de predicción normalizado (suma del error de predicción dividido por la varianza de respuesta) para los 'mejores' modelos CAR para BET y SKJ para 2010-2021, para datos de buques de clases 1-5 (lances OBJ). Los valores menores de 1 indican un buen desempeño de predicción.

Vessel size class 1-5	2010	2011	2012	2013	2014	2015	2016	2017	2018	2019	2020	2021
BET												
proportion of variance explained	0.88	0.97	0.94	0.98	0.84	0.95	0.95	0.96	0.97	0.97	0.97	0.96
normalized prediction error	0.8	0.35	0.4	0.18	0.93	0.56	0.29	0.31	0.33	0.24	0.19	0.21
SKJ												
proportion of variance explained	0.91	0.97	0.97	0.98	0.97	0.95	0.95	0.99	0.99	0.99	0.99	0.87
normalized prediction error	0.51	0.25	0.17	0.09	0.23	0.61	0.39	0.24	0.04	0.11	0.15	0.3

TABLE 6. Correlation coefficients of the CAR estimates with the BSE for 2010-2019 for the three species of tuna using the short-term and long-term models. The 'best' model is marked in bold. The following correction was made to the CAR estimates: updated to reflect the latest total fleet catch of tropical tunas.
TABLA 6. Los coeficientes de correlación de las estimaciones CAR con la BSE para 2010-2019 para las tres especies de atunes utilizando los modelos de corto y largo plazo. El 'mejor' modelo está marcado en negrita. Se realizó la siguiente corrección en las estimaciones CAR: se actualizaron para reflejar la captura total más reciente de la flota de atunes tropicales.

Correlation coefficients	2010-2019 BET	2010-2019 SKJ	2010-2019 YFT
Short-term model	0.70	0.98	0.92
Long-term model	**0.78**	**0.98**	**0.95**

TABLE 7. Absolute (in metric tons) and percent bias of the BSE in 2020-2021 as estimated from the best CAR model. Bias is defined as the BSE estimate minus the CAR estimate, divided by the CAR estimate. The following correction was made to the 2020-2021 CAR estimates: updated to reflect the latest total fleet catch of tropical tunas.
TABLA 7. Sesgo absoluto (en toneladas métricas) y porcentual de la BSE en 2020-2021 según la estimación del mejor modelo CAR. El sesgo se define como la estimación BSE menos la estimación CAR, dividido por la estimación CAR. Se realizó la siguiente corrección en las estimaciones CAR de 2020-2021: se actualizaron para reflejar la captura total más reciente de la flota de atunes tropicales.

Bias	**2020**	**2021**
BET	8,307 (12%)	8,773 (18%)
SKJ	1,156 (0.6%)	-14,560 (-6%)
YFT	-9,463 (-18%)	5,787 (10%)

TABLE 8. OBJ estimates for BSE program divided by CAR model, for 2020-2021 for the three species of Tuna. The following correction was made to the 2020-2021 CAR estimates: updated to reflect the latest total fleet catch of tropical tunas.
TABLA 8. Estimaciones OBJ del programa BSE divididas por el modelo CAR, para 2020-2021, para las tres especies de atunes. Se realizó la siguiente corrección en las estimaciones CAR de 2020-2021: se actualizaron para reflejar la captura total más reciente de la flota de atunes tropicales.

Ratio	**2020**	**2021**
BET	1.12	1.18
SKJ	1.00	0.94
YFT	0.82	1.10

TABLE 9. Correlation of BSE with the best CAR models for the three Tuna species in 2010-2019. The following correction was made to the CAR estimates: updated to reflect the latest total fleet catch of tropical tunas.
TABLA 9. Correlación de la BSE con los mejores modelos CAR para las tres especies de atunes en 2010-2019. Se realizó la siguiente corrección en las estimaciones CAR: se actualizaron para reflejar la captura total más reciente de la flota de atunes tropicales.

Correlation coefficients	2010-2019 BET	2010-2019 SKJ	2010-2019 YFT
Best CAR model	0.78	0.98	0.95
Best CAR model with trips excluded mimicking 2020 pandemic data loss situation	0.73	0.98	0.92

APPENDIX A: STATISTICAL MODELING

In our modeling we have tested for different choices of spatio-temoral CAR model with adjacency matric ***W*** as described below:

In Figure A1, we have used the *traditional method* to define ***W*** from the physical maps of the regions which give us a spatial matrix map with an adjacency matrix of the form. In the left panel of the figure, we represent this using a colored matrix. The yellow values denote 1 or direct adjacency and the whites denote 0 or no direct adjacency. In the arrow map (right panel), the substitution rules are represented by red arrows. The arrows denote adjacency of the binary **W** matrix, so $w_{jk} = w_{kj} = 1$ if *j*-th and *k*-th regions share boundaries or corners. The result by running this model on the data for OBJ set types is given in the Appendix. In our preliminary analysis, we have also used the traditional method to define ***W*** from the physical maps of the regions which give us a spatial matrix map with an adjacency matrix of the form – but we removed the diagonal areas from the adjacency matrix. The yellow values denote 1 or direct adjacency and the whites denote 0 or no direct adjacency.

	1	2	3	4	5	6	7	8	9	10	11	12	13
1	0	1	0	1	0	0	0	1	0	1	0	0	0
2	1	0	1	1	0	0	0	1	0	1	0	0	0
3	0	1	0	1	1	0	0	0	1	1	0	0	0
4	1	1	1	0	1	0	0	0	0	0	0	0	0
5	0	0	1	1	0	1	1	0	1	0	0	0	0
6	0	0	0	0	1	0	1	0	0	0	0	1	1
7	0	0	0	0	1	1	0	0	1	0	0	1	1
8	1	1	0	0	0	0	0	0	0	0	0	0	0
9	0	0	1	0	1	0	1	0	0	1	1	1	0
10	1	1	1	0	0	0	0	0	1	0	1	0	0
11	0	0	0	0	0	0	0	0	1	1	0	1	0
12	0	0	0	0	0	1	1	0	1	0	1	0	1
13	0	0	0	0	0	1	1	0	0	0	0	1	0

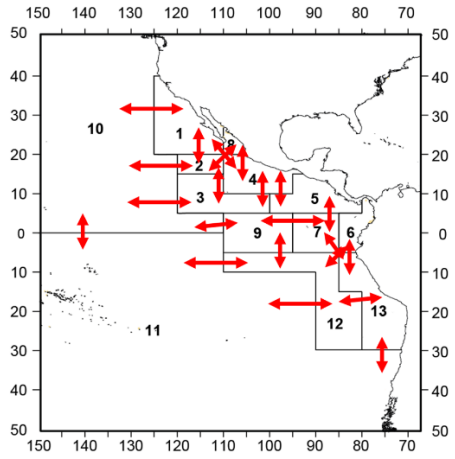

FIGURE A1. W or adjacency/neighborhood matrix of the traditional model in spatio-temporal CAR models through a matrix (left) and through arrows (right).

In Figure A2, we represent the model with a certain adjacency matrix where the adjacency is defined when the regions share boundaries but not corners. Again, as in FigureA1 (right panel) the substitution rules are represented by red arrows. The arrows denote adjacency of the binary W matrix, so $w_{jk} = w_{kj} = 1$ if j-th and k-th regions share boundaries (but not corners). The results corresponding to the modeling where temporal units were chosen to be years were not very good. We modeled the BET using the model but discontinued observing the poor performance of the model defined by poor consistency with the BSE estimates.

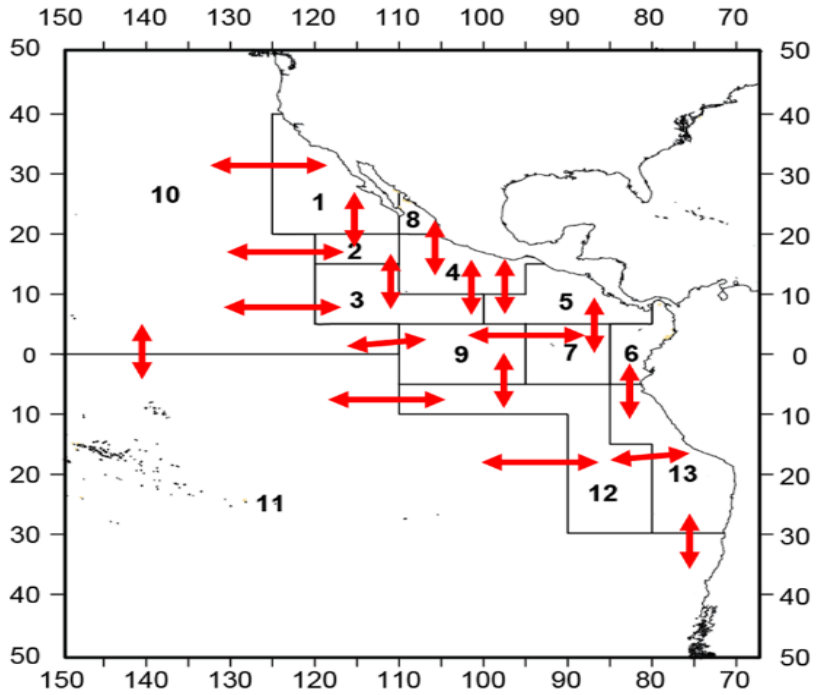

FIGURE A2. W or adjacency/neighborhood matrix of the traditional model having got rid of the diagonal adjacencies in spatio-temporal through arrows (right).

Building areal models with no temporal component

Although the spatial structure seen in the p_{kt} (Figures 2,3,4) may be modelled by known predictor variables in a regression model, as was done in the exploratory analyses, it is common for spatial structure to remain in the residuals. The most common remedy for this residual autocorrelation is to augment the linear predictor with a set of spatially autocorrelated random effects, as part of a Bayesian hierarchical model. These random effects are typically represented with a conditional autoregressive (CAR, Besag *et al.* 1991) prior, which induces spatial autocorrelation through the adjacency structure of the areal units. However, these CAR priors force the random effects to exhibit a single global level of spatial autocorrelation, ranging from independence through to strong spatial smoothness. Such a uniform level of spatial autocorrelation for the entire EPO may be unrealistic, given the spatial variation seen in p_{kt} (Figure 4).

A number of approaches have been proposed for extending the class of CAR priors to deal with localized spatial smoothing amongst the random effects, including Lee and Mitchell (2012), and Lee and Sarran (2015). These types of models are typically implemented in a Bayesian setting, where inference is based on Markov chain Monte Carlo (MCMC) simulation. Some of the choices we considered are

Univariate Model with Gaussian assumption

Model

$$\log(p_s) = Y_s$$

$$Y_s \mid \mu_s \sim Normal\ (\mu_s, \nu^2\ )$$
$$\mu_s = X^T\beta + \psi_s$$

Here ψ_s is the spatially autocorrelated component.

Priors

$$\beta \sim N(\mu_\beta, \Sigma_\beta)$$

$$\nu^2 \sim \text{Inverse-Gamma}(a, b).$$

For the spatial model with no temporal component the following was a special case to incorporate the latent spatial effects ψ_s into a hierarchical model structure.

S.CARleroux model: Leroux *et al.* (2000) proposed the following alternative Conditional Autoregressive (CAR) prior for modeling varying strengths of spatial autocorrelation using only a single set of random effects. **W** is the symmetric neighborhood matrix so that W_{ik} give the weights of the strength of the spatial association between the i'th and k'th regions when they are "neighbors". The only condition we need are the row totals of **W** add up to a positive value. And ϕ_k are the spatially autocorrelated components.

$$\psi_k = \phi_k$$

$$\Phi_k \mid \Phi_{-k}, \boldsymbol{W}, \tau^2, \rho \sim N\left(\frac{\rho \sum_i w_{ki} \phi_i}{\rho \sum_i w_{ki} + 1 - \rho}, \frac{\tau^2}{\rho \sum_i w_{ki} + 1 - \rho}\right)$$

$$\rho \sim Unif(0, 1)$$

$$\tau^2 \sim Inverse\ Gamma(a, b)$$

Thus, ρ represents overall spatial autocorrelation in the model, where as τ^2 represents the overall spatial variance. In the model the traditional adjacency matrix W defined in Appendix A (i) was used.

APPENDIX B: ESTIMATES AND PERFORMANCE MEASURES

Apart from numerical values, we have also used some other performance measures for model screening of the CAR models discussed in the paper and in Appendix A, namely (i) Normal Quantile-Quantile plots of the residuals, (ii) fitted versus observed plots. Additionally, for each candidate CAR model – we have used two options: (i) autoregressive (1) or AR (1) versus (ii) autoregressive (2) or AR (2). We observed that AR (1) was a better choice in each case, and so the results quoted below pertain to AR (1).

Below we provide the catch estimates and model performance of different models we have built, tested, and compared results with the BSE through 2010-2019. The results of the model can be summarized as follows –estimates of the species composition are given in the first, and performance measures are given in the consecutive table below the first.

TABLE B1. Model performance with W chosen to be `traditional' adjacency matrix for 13 regions, using annual data. The difference with the `best' CAR model is that the W is given as in Figure A1:

Year	2010	2011	2012	2013	2014	2015	2016	2017	2018	2019	2020
Vessel size class 6											
BET											
proportion of variance explained	0.97	0.93	0.9	0.91	0.95	0.99	0.999	0.98	0.98	0.88	0.76
normalized prediction error	0.41	0.58	0.93	0.77	0.75	0.13	0.09	0.42	0.29	0.98	1.41
SKJ											
proportion of variance explained	0.59	0.45	0.78	0.64	0.64	0.39	0.38	0.47	0.41	0.42	0.47
normalized prediction error	2.37	0.73	3.9	1.71	1.27	1	1.5	1.15	0.75	1.18	1.59
vessel size class 1-5											
BET											
proportion of variance explained	0.57	0.91	0.75	0.8	0.97	0.99	0.99	0.65	0.8	0.92	0.7
normalized prediction error	1.7	0.87	1.21	1.72	0.4	0.09	0.12	1.21	1.61	0.87	1.24
SKJ											
Proportion of variance explained	0.67	0.97	0.99	0.99	0.49	0.6	0.77	0.32	0.25	0.24	0.59
normalized prediction error	0.93	0.23	0.11	0.18	2	1.92	0.49	1.37	1.4	1.69	1.79

TABLE B2. Model performance with W chosen to be `traditional' adjacency matrix for 13 regions, using quarterly data. The difference with the 'best' CAR model is that the W is given by Figure A1 and the data was aggregated on quarters, and not years.

OBJ sets **Vessel size class 6** **Year**	**2010**	**2011**	**2012**	**2013**	**2014**	**2015**	**2016**	**2017**	**2018**	**2019**	**2020**
BET											
proportion of variance explained	0.866	0.85	0.87	0.9	0.89	0.91	0.91	0.91	0.92	0.95	0.9
normalized prediction error	8.11	6.95	7.35	7.83	6.84	7.91	7.3	7.8	6.28	9.56	11.54
SKJ											
proportion of variance explained	0.866	0.85	0.87	0.9	0.89	0.91	0.91	0.91	0.92	0.95	0.9
normalized prediction error	8.11	6.95	7.35	7.83	6.84	7.91	7.3	7.8	6.28	9.56	11.54
vessel size class 1-5											
BET											
proportion of variance explained	0.9	0.89	0.9	0.88	0.85	0.94	0.99	0.98	0.93	0.88	0.94
normalized prediction error	1.4	1.6	2.95	3.03	2.73	1.51	0.56	1.19	1.52	1.78	0.89
SKJ											
proportion variance explained	0.9	0.89	0.9	0.88	0.85	0.94	0.99	0.98	0.93	0.88	0.94
normalized prediction error	1.4	1.6	2.95	3.03	2.73	1.51	0.56	1.19	1.52	1.78	0.89

TABLE B3. Model performance from CAR model with W mimicking BSE substitution rules for 13 regions, using quarterly data. This is the like the 'best' CAR model we used; however, the data that was used was aggregated over quarters instead of years:

OBJ sets **Year**	**2010**	**2011**	**2012**	**2013**	**2014**	**2015**	**2016**	**2017**	**2018**	**2019**	**2020**
vessel size class 6											
BET											
proportion of variance explained	0.9	0.9	0.91	0.96	0.92	0.93	0.9	0.9	0.92	0.99	0.99
normalized prediction error	1.96	1.98	2	2.02	2.55	1.72	2.47	2.32	1.39	0.63	0.42
SKJ											
proportion of variance explained	0.69	0.73	0.71	0.83	0.75	0.81	0.85	0.93	0.94	0.89	0.93
normalized prediction error	4.04	2.53	4.2	3.34	3.89	1.66	1.67	2.24	2.18	1.79	1.57
vessel size class 1-5											
BET											
proportion of variance explained	0.94	0.93	0.95	0.89	0.97	0.99	0.997	0.998	0.995	0.98	0.88
normalized prediction error	1.4	1.32	2.19	2.85	1.22	0.63	0.3	0.39	0.39	0.71	1.88
SKJ											
proportion of variance explained	0.78	0.87	0.88	0.96	0.96	0.98	0.59	0.7	0.62	0.48	0.78
normalized prediction error	3.5	0.36	2.03	2.03	1.07	0.91	7.66	6.13	1.53	2.98	2.75

TABLE B4. Model performance from CAR model with W mimicking BSE substitution rules for 13 regions, with annual data (short-term model). This is the like the 'best' CAR model we used; however, the number of years used in the model was three instead of five:

OBJ sets **Year**	**2010**	**2011**	**2012**	**2013**	**2014**	**2015**	**2016**	**2017**	**2018**	**2019**	**2020**
vessel size class 6											
BET											
proportion of variance explained	1	0.98	0.98	0.97	0.96	1	0.99	1	0.99	0.99	0.93
normalized prediction error	0.54	0.38	0.48	0.49	0.73	0.12	0.11	0.14	0.22	0.17	0.75
SKJ											
proportion of variance explained	1	0.92	0.99	0.86	0.76	0.89	0.95	0.93	0.92	0.9	0.86
normalized prediction error	0.14	0.81	0.38	0.99	1.04	0.78	1.06	0.62	0.67	0.98	1.28
vessel size class 1-5											
BET											
proportion of variance explained	0.88	0.98	0.9	0.92	0.85	0.93	0.94	0.96	0.96	0.93	0.97
normalized prediction error	0.79	0.27	0.34	0.34	0.82	0.63	0.32	0.35	0.41	0.34	0.19
SKJ											
proportion of variance explained	0.91	0.89	0.98	0.81	0.9	0.85	0.87	0.92	0.89	0.87	0.99
normalized prediction error	0.5	0.42	0.04	0.19	0.42	1.01	0.62	1.1	0.13	0.43	0.15

TABLE B5. Model performance from best CAR model with trips excluded at Manta, Mazartan, Pasorja (April-December for all years) mimicking the pandemic situation (see Appendix A):

OBJ sets **Year**	**2010**	**2011**	**2012**	**2013**	**2014**	**2015**	**2016**	**2017**	**2018**	**2019**	**2020**	**2021**
vessel size class 6												
BET												
proportion of variance explained	0.99	0.99	0.98	0.95	0.96	0.95	0.99	0.99	0.99	0.99	0.99	0.99
normalized prediction error	0.36	0.19	0.52	0.63	0.77	0.91	0.15	0.19	0.12	0.1	0.14	0.19
SKJ												
proportion of variance explained	1	0.82	0.78	0.87	0.83	0.79	0.74	0.84	0.83	0.85	0.88	1
normalized prediction error	0.2	1.35	2.9	1.18	0.68	1.03	2.22	0.9	0.97	0.59	0.62	0.19
vessel size class 1-5												
BET												
proportion of variance explained	0.88	0.97	0.94	0.98	0.84	0.95	0.95	0.96	0.97	0.97	0.97	0.96
normalized prediction error	0.8	0.35	0.4	0.18	0.93	0.56	0.29	0.31	0.33	0.24	0.19	0.21
SKJ												
proportion of variance explained	0.91	0.97	0.97	0.98	0.97	0.95	0.95	0.99	0.99	0.99	0.99	0.87
normalized prediction error	0.51	0.25	0.17	0.09	0.23	0.61	0.39	0.24	0.04	0.11	0.15	0.3

Next, we provide the correlation coefficients between the CAR estimates and the BSE for the three species (BET, SKJ, YFT). We have calculated correlations twice—once for the years 2010-2019, and once for 2010-2020.

TABLE B6. Correlation of CAR estimates with BSE; the 'best' CAR model results are marked in bold. The following correction was made to the CAR estimates: updated to reflect the latest total fleet catch of tropical tunas.

Correlation coefficients	**2010-2020 BET**	**2010-2019 BET**	**2010-2020 SKJ**	**2010-2019 SKJ**	**2010-2020 YFT**	**2010-2019 YFT**
Traditional W with year as temporal unit	.80	0.59	0.98	0.99	0.97	0.96
Traditional W with quarters as temporal unit	0.68	0.34	0.97	0.99	.84	.93
W mimicking BSE substitution quarters as temporal units	0.76	0.43	0.89	.92	0.69	0.80
W mimicking BSE substitution with year as temporal unit (Short-term model)	0.52	0.70	0.98	0.98	0.85	0.92
W mimicking BSE substitution with year as temporal unit (Long-term model)	**0.83**	**0.78**	**0.98**	**0.98**	**0.95**	**0.95**

TABLE B7. Correlation of BET CAR estimates with BSE for various CAR models, the 'best' CAR Model results is marked in bold fonts. The following correction was made to the CAR estimates: updated to reflect the latest total fleet catch of tropical tunas.

Correlation coefficient	**2010-2020**	**2010-2019**
Traditional W with year as temporal unit	0.80	0.59
Traditional W with year as temporal unit remove the diagonals from W	-0.08	0.39
Traditional W with quarters as temporal unit	0.68	0.34
Modified W with quarters as temporal units	0.76	0.43
Modified W with year as temporal unit (short term)	0.52	0.70
Modified W with year as temporal unit (long-term)	**0.83**	**0.78**
Spatial CAR with no temporal term, with traditional W	0.15	0.18

TABLE B8a. Parameter estimates of the BET and SKJ 'best' CAR model for vessel size 6.

BET	**vessel 6**						**SKJ**					
Parameters	Intercept	Slope	tau2	nu2	rho.S	rho.T	Intercept	Slope	tau2	nu2	rho.S	rho.T
2010	0.27	1.25	0.03	0.07	0.66	0.45	0.54	2.41	0.05	0.01	0.72	0.92
2011	0.47	1.34	0.03	0.05	0.65	0.48	-0.03	1.08	0.01	0.03	0.45	0.42
2012	0.25	1.20	0.01	0.25	0.49	0.30	0.31	1.96	0.02	0.31	0.58	0.42
2013	-0.16	1.06	0.05	0.02	0.74	0.83	0.38	2.16	0.02	0.13	0.57	0.30
2014	-0.28	1.06	0.05	0.01	0.83	0.90	0.46	2.38	0.01	0.50	0.49	0.32
2015	-0.16	1.06	0.05	0.02	0.74	0.83	0.38	2.15	0.02	0.13	0.55	0.30
2016	-0.28	1.06	0.06	0.01	0.82	0.90	0.46	2.38	0.01	0.51	0.46	0.34
2017	-0.47	1.05	0.08	0.02	0.80	0.71	0.32	1.80	0.01	0.09	0.36	0.20
2018	-0.99	0.85	0.08	0.02	0.82	0.65	0.38	1.98	0.01	0.08	0.42	0.23
2019	-0.43	1.01	0.06	0.02	0.76	0.46	-0.06	0.85	0.01	0.01	0.31	0.35
2020	-0.02	1.13	0.02	0.29	0.60	0.39	-0.06	0.99	0.01	0.01	0.29	0.39
2021	-0.26	1.06	0.05	0.02	0.77	0.38	0.22	1.69	0.03	0.01	0.70	0.92

TABLE B8b. Parameter estimates of the BET and SKJ 'best' CAR model for vessel size 1-5.

BET	vessel type 1-5						**SKJ**					
Parameters	Intercept	Slope	tau2	nu2	rho.S	rho.T	Intercept	Slope	tau2	nu2	rho.S	rho.T
2010	-0.67	0.88	0.03	0.71	0.61	0.35	0.08	1.66	0.02	0.10	0.58	0.32
2011	-0.92	0.84	0.06	0.04	0.82	0.45	-0.08	1.09	0.03	0.04	0.66	0.34
2012	-1.03	0.82	0.07	0.04	0.80	0.41	-0.05	1.08	0.03	0.03	0.73	0.35
2013	-1.12	0.82	0.09	0.03	0.82	0.45	-0.03	1.09	0.03	0.03	0.71	0.34
2014	-1.15	0.83	0.03	0.52	0.71	0.33	0.01	1.10	0.04	0.02	0.69	0.33
2015	-1.56	0.72	0.07	0.06	0.81	0.37	0.00	1.13	0.03	0.05	0.66	0.29
2016	-1.60	0.73	0.07	0.05	0.81	0.40	0.02	1.16	0.02	0.07	0.62	0.28
2017	-1.65	0.73	0.09	0.05	0.79	0.42	-0.14	0.72	0.05	0.02	0.84	0.82
2018	-1.65	0.72	0.09	0.03	0.84	0.36	-0.14	0.62	0.06	0.02	0.80	0.56
2019	-1.71	0.72	0.06	0.03	0.87	0.31	-0.15	0.63	0.05	0.02	0.84	0.53
2020	-1.75	0.71	0.06	0.06	0.81	0.32	-0.17	0.61	0.06	0.02	0.83	0.57
2021	-1.99	0.66	0.09	0.04	0.74	0.32	-0.15	0.63	0.02	0.14	0.65	0.25

APPENDIX C

DATA SOURCES

The primary three data sources are (i) Observer data, (ii) Logbook data (iii) Cannery data and (iv) Port-sampling data and are described below.

Observer data

These data are collected by observers on board large (IATTC Class-6; > 363 mt fish carrying-capacity) vessels, for which data collection began in 1980 and there has been 100% observer coverage (or nearly so) since 1992. To note, however, is that detailed observer data are only available on the IATTC database for all Class-6 trips since 2009; data of trips of Mexican-flag vessels sampled by the Mexican national observer program are not available on the database for years prior to 2009, although logbook data are available for many of these trips (see below). Observer data are also available for a small percentage of trips of small (IATTC Classes 1-5; ≤ 363mt) purse-seine vessels.

Observers collect data on fishing activities, gear characteristics, and catch of target and non-target species (non-target species are also referred to as 'bycatch', e.g., billfish species, dorado, turtles, marine mammals, etc.). For catch of both target and non-target species, size composition is recorded. However, the type of size data collected depends on the taxonomic group; size data for the tropical tuna species are only amounts of catch by three weight categories ('small': fish < 2.5 kg total weight; 'medium': fish between 2.5 kg and 15 kg; 'large': fish > 15 kg), not actual measurements of length or weight of individual fish. The observer data have the finest spatial and temporal resolution of any of the four main data sources, with a spatial resolution of 100th of a degree (decimal degrees) and a temporal resolution of minutes to hours (depending on the fishing activity). One important difference between the catch data collected by observers and that abstracted from vessel logbooks (see below) is that logbooks contain only the amount of catch loaded into the wells of the specific vessel, whereas observers record several catch quantities: the amount of tuna caught (sometimes referred to as 'catch weights' or 'capture'); the amount of tuna loaded onto the vessel (referred to as 'load weights'); and, the amount of tuna discarded. (Discarding of fish has been prohibited in recent years, however.) The amount of tuna 'retained', which is the difference between the capture and the discards, includes any tuna catch given to another vessel or transferred to storage pens, in addition to the amount of tuna catch loaded into the vessel's wells. Thus, the only the loaded catch can be compared between observer data and logbook data.

For a comprehensive description of observer data held at IATTC, see Fuller *et al*. (2022).

Logbook data

Logbook data are data abstracted by IATTC staff from fishermen's logbooks on fishing locations, dates, types of purse-seines sets, and target species catch amounts (no size information is available). The logbook data on catches (load weights only) are set-by-set data, at a spatial resolution of 100th of a degree (decimal degrees). The data are available for all size classes of purse-seine vessels but are typically not used for fishing trips for which observer data are also available because the logbook data are more limited in scope. The coverage of the logbook database has improved over time and a timeline can be found in Document SAC-08-06a (which also contains a useful description of the types of data available for Class 1-5 purse-seine vessels).

Cannery data

Cannery data are catch amounts of target species by trip, provided to the IATTC staff by tuna canneries. They are trip-level data, without any information on exact fishing locations or dates or operational characteristics (e.g., purse-seine set type), although information on fishing zones and trip departure and

arrival dates are provided. No size information is currently available on the IATTC database; some canneries do provide estimates of catch by weight categories, but those categories differ among canneries, making the size information problematic to use for catch composition estimation Cannery data are not available to IATTC staff for all trips nor from all canneries.

Port-sampling data

The port-sampling data are collected by IATTC field office staff when purse-seine vessels unload their catch in port. The data are samples of the catch from one or more wells (fish storage compartments on board the vessel); staff typically try to sample only one or two wells of a trip, rather than all wells of the trip that meet the sampling criteria (see below). The data collected include length measurements from a sample of fish, and, separately from the fish measured, counts of species from another sample of fish. The sampling protocol that is to be followed by the staff can be found in the appendix of Suter (2010). Very generally, the protocol requires samplers to alternate between counting and measuring fish (in groups of 25 fish for counts and 50 fish for measurements), with the purpose of extending each type of sampling over a larger fraction of the unloading than would occur if the counts and measurements were each collected from a contiguous number of fish. The port-sampling data can be linked to observer and/or logbook data through trip and vessel identifiers.

The port-sampling data have a coarse spatial and temporal resolution. Since 2000, all samples can be assigned to a 5° square area. A monthly resolution is likely the smallest temporal resolution that can be assigned to all samples. In principle, for some percentage of samples, it is possible to obtain finer spatial and temporal resolution. However, this is only in cases where, for example, an entire set fills the well that was sampled; wells on the vessel can contain samples from multiple sets and the catch of one set may be loaded into multiple wells. The sampling instructions stipulate that sampled wells must have catch from the same purse-seine set type, sampling area (Figure 7) and month. Wells with catch from different set types/sampling areas/months are not sampled.

Not every trip is sampled by the port-sampling program, and the coverage of trips differs by vessel size class (see last slides of this presentation). Although the coverage computed in terms of sampled trips is relatively high (at least for Class-6 vessels), the coverage in terms of the percentage of wells sampled or percentage of the catch sampled is low; an added consideration when considering the percentage of wells sampled is that not all wells would be considered sampleable under the current protocol, as noted above. The percentage of trips sampled is determined by resources available and logistical constraints, rather than being established to achieve a specific precision for the estimates of catch. Some vessels unload in locations where it is not possible to sample their catch in port.

The sampling protocol has changed over time. Prior to 2000 the sampling was only for the length composition of the catch. Beginning in 2000, sampling was also for species composition. The sampling has always been a multi-stage protocol, where first a fishing trip and then a well (or wells) of that trip of are selected for sampling, and then fish within the well are selected. It is worth noting that although the instructions to samplers (appendix of Suter 2010) imply that selection of units for sampling is at random, when in actuality, the selection of trips to sample is largely opportunistic (as is selection of wells, from among those wells of a trip that meet the same area/month/set type criteria), and the sampling of fish within a well most closely resembles a single-cluster systematic sample (but not initiated from a random start).

CURRENT CATCH COMPOSITION ESTIMATION METHODOLOGY

A description of the statistical methodology used since 2000 to estimate the purse-seine tuna catch composition for the three target tuna species can be found in several documents: starting on page 339 of Stock Assessment Report 2; starting on page 311 of Stock Assessment Report 4; and, for both time periods (1975-1999 and 2000 onwards), in Document BET-02-06 . The latter document also contains a description of the data used for catch-estimation and stock assessments.

The methodology is a design-based approach to catch estimation, as opposed to a model-based approach. The methodology amounts to estimation of catch composition using a type of ratio estimator of species and size composition, which is applied to the port-sampling data, by strata. Equations can be found in the documents noted in the previous paragraph. In practical terms, the methodology can be broken down into the following three steps:

1) Obtain the total purse-seine fleet catch of tropical tunas (that is find the total of yellowfin, bigeye and skipjack). This total is based on catches from: cannery data, observer data (load weights; if no cannery data for a trip are available), and logbook data (if no cannery or observer data are available for a trip).

2) Distribute the total from (1) to strata (area x month x set type x vessel size class category (Classes 1-5; Class-6)), using the proportion of total tropical tuna catch in each stratum (proportions computed from the combination of observer and logbook data).

3) For each stratum, distribute the total tropical tuna catch total from (2) to species and size (1 cm length bins), using estimates of the species and size composition of the catch from the port-sampling data. Because there are always strata with catch but no port-sampling data, species and size composition in some strata are based on port-sampling data from 'neighboring' strata. Briefly, the 'best' neighboring stratum to a stratum without port-sampling data is determined through a set of hierarchical rules. In general, priority is given to set type – which means that to the extent possible, the 'neighbor' stratum should have the same set type. Then priority is given to month and area, and finally to vessel size class category. For example, a stratum that has catch from OBJ sets in area 7, month 3, and Class-6 vessels, would be considered 'closer' to a stratum with catch from OBJ sets in the area 7 and month 3 but from Class 1-5 vessels than to a stratum with catch from OBJ sets in area 9 and month 3 and Class-6 vessels.